HAL
open science

Upper Cretaceous exhumation of the western Rhodope Metamorphic Province (Chalkidiki Peninsula, northern Greece)

Konstantinos Kydonakis, Kerry Gallagher, Jean-Pierre Brun, Marc Jolivet, Frédéric Gueydan, Dimitrios Kostopoulos

To cite this version:

Konstantinos Kydonakis, Kerry Gallagher, Jean-Pierre Brun, Marc Jolivet, Frédéric Gueydan, et al.. Upper Cretaceous exhumation of the western Rhodope Metamorphic Province (Chalkidiki Peninsula, northern Greece). Tectonics, 2014, 33 (6), pp.1113-1132. 10.1002/2014TC003572 . insu-01053579

HAL Id: insu-01053579

https://insu.hal.science/insu-01053579v1

Submitted on 31 Jul 2014

HAL is a multi-disciplinary open access archive for the deposit and dissemination of scientific research documents, whether they are published or not. The documents may come from teaching and research institutions in France or abroad, or from public or private research centers.

L'archive ouverte pluridisciplinaire **HAL**, est destinée au dépôt et à la diffusion de documents scientifiques de niveau recherche, publiés ou non, émanant des établissements d'enseignement et de recherche français ou étrangers, des laboratoires publics ou privés.

AGU PUBLICATIONS

Tectonics

RESEARCH ARTICLE

10.1002/2014TC003572

Key Points:
- The Vertiskos Unit is the westernmost part of the Rhodope Metamorphic Province
- Fission track analysis implies Upper Cretaceous exhumation of the Vertiskos Unit
- Our work establishes the Vertiskos Unit as the oldest exhumed basement of Greece

Supporting Information:
- Readme
- Figure S1
- Figure S2

Correspondence to:
K. Kydonakis,
konstantinos.kydonakis@univ-rennes1.fr

Citation:
Kydonakis, K., K. Gallagher, J.-P. Brun, M. Jolivet, F. Gueydan, and D. Kostopoulos (2014), Upper Cretaceous exhumation of the western Rhodope Metamorphic Province (Chalkidiki Peninsula, northern Greece), *Tectonics*, *33*, doi:10.1002/2014TC003572.

Received 4 MAR 2014
Accepted 9 MAY 2014
Accepted article online 22 MAY 2014

Upper Cretaceous exhumation of the western Rhodope Metamorphic Province (Chalkidiki Peninsula, northern Greece)

Konstantinos Kydonakis[1], Kerry Gallagher[1], Jean-Pierre Brun[1], Marc Jolivet[1], Frédéric Gueydan[2], and Dimitrios Kostopoulos[3]

[1]Géosciences Rennes, UMR 6118 CNRS, Rennes, France, [2]Géosciences Montpellier, UMR 5243 CNRS, Montpellier, France, [3]Faculty of Geology and Geoenvironment, National and Kapodistrian University of Athens, Athens, Greece

Abstract The Vertiskos Unit of northern Greece is an elongated basement belt with a complex poly-metamorphic history. It extends from Greece (Chalkidiki peninsula), to the south, up to Serbia, in the north, and arguably represents the westernmost part of the Rhodope Metamorphic Province (northern Greece to southern Bulgaria). The Vertiskos Unit experienced a medium pressure lower amphibolite-facies metamorphic overprint during the Alpine Orogeny. The available medium-temperature geochronology implies that it remained at temperature of approximately 300°C (or slightly higher) during Lower Cretaceous. In order to constrain its post-Lower Cretaceous thermal history, until near-surface exposure, we applied apatite fission track analysis. The central ages obtained range from 68.5 ± 3.8 to 46.6 ± 3.6 Ma (uppermost Cretaceous to Middle Eocene) and mean track lengths between 13 and 13.5 μm. We applied two inverse thermal modeling approaches using either each sample independently (high degree of freedom in the thermal history, better data fit) or all samples together interpreting them as a vertical profile (simpler thermal history, worse data fit). Irrespective of the modeling approach, we conclude that the bulk thermal history of the Vertiskos Unit crosses the high-temperature limit of the apatite partial annealing zone by the uppermost Cretaceous and reaches near-surface conditions as early as lower/middle Eocene. These results contrast with the thermal history of the other domains of the Rhodope Metamorphic Province further east (namely the Southern Rhodope Core Complex and the Northern Rhodope Complex) and establish the Vertiskos basement complex as the oldest exhumed coherent basement fragment of the Rhodope Metamorphic Province and Greece.

1. Introduction

The northeastern part of Greece and southwestern part of Bulgaria is known as the Rhodope Metamorphic Province [see *Burg*, 2012, and references therein] (Figure 1). It constitutes an extended tectonic element between two Alpine Mountain Chains: the Carpathians-Balkanides to the north and the Dinarides-Hellenides to the south. Widespread Jurassic-Cretaceous metamorphic ages [*Reischmann and Kostopoulos*, 2002; *von Quadt et al.*, 2008, 2009; *Krenn et al.*, 2010; *Nagel et al.*, 2011; *Liati et al.*, 2011, and references therein], roughly corresponding to eclogites-facies peak event and subsequent amphibolite-facies overprint, have been described for the whole domain in the literature. The final unroofing, as estimated by low-temperature thermochronology, for the central and northeastern parts is well defined at Eocene-Miocene [e.g., *Hejl et al.*, 1998, 2010; *Wuthrich*, 2009]. Regardless, the cooling history of the westernmost part of the Rhodope Metamorphic Province, known as the Serbo-Macedonian Domain, remains poorly constrained.

Apatite and zircon fission track (AFT, ZFT) analysis is often adopted for determining low-temperature thermal events. A general overview of the basic methodology is given in *Gallagher et al.* [1998] and many different FT applications has been reported in the literature over the past few decades such as investigation of the thermal evolution of basement rocks and sedimentary basins [e.g., *Leech and Stockli*, 2000; *Barbarand et al.*, 2001; *Foster and Raza*, 2002; *Jolivet et al.*, 2007; *Labaume et al.*, 2008; *Balestrieri et al.*, 2011; *Sanchez et al.*, 2011; *Sahu et al.*, 2013; *Yang et al.*, 2013], passive margin denudation history [e.g., *Gunnell et al.*, 2003; *Yi et al.*, 2009; *Cogne et al.*, 2011, 2012; *Dörr et al.*, 2012], detritus supply and provenance studies [e.g., *Carter*, 1999; *Bernet and Garver*, 2005; *Carrapa*, 2009; *Wang et al.*, 2011; *Balestrieri et al.*, 2013]. Apatite FT age data are best coupled with spontaneous track length measurement allowing for the determination of a relatively detailed low-temperature thermal history (T-t). The method can be applied to rocks that have previously been annealed at temperature above the apatite partial annealing zone (PAZ; ~120°C; dependence on the crystal composition) [*Donelick et al.*,

©2014. American Geophysical Union. All Rights Reserved.

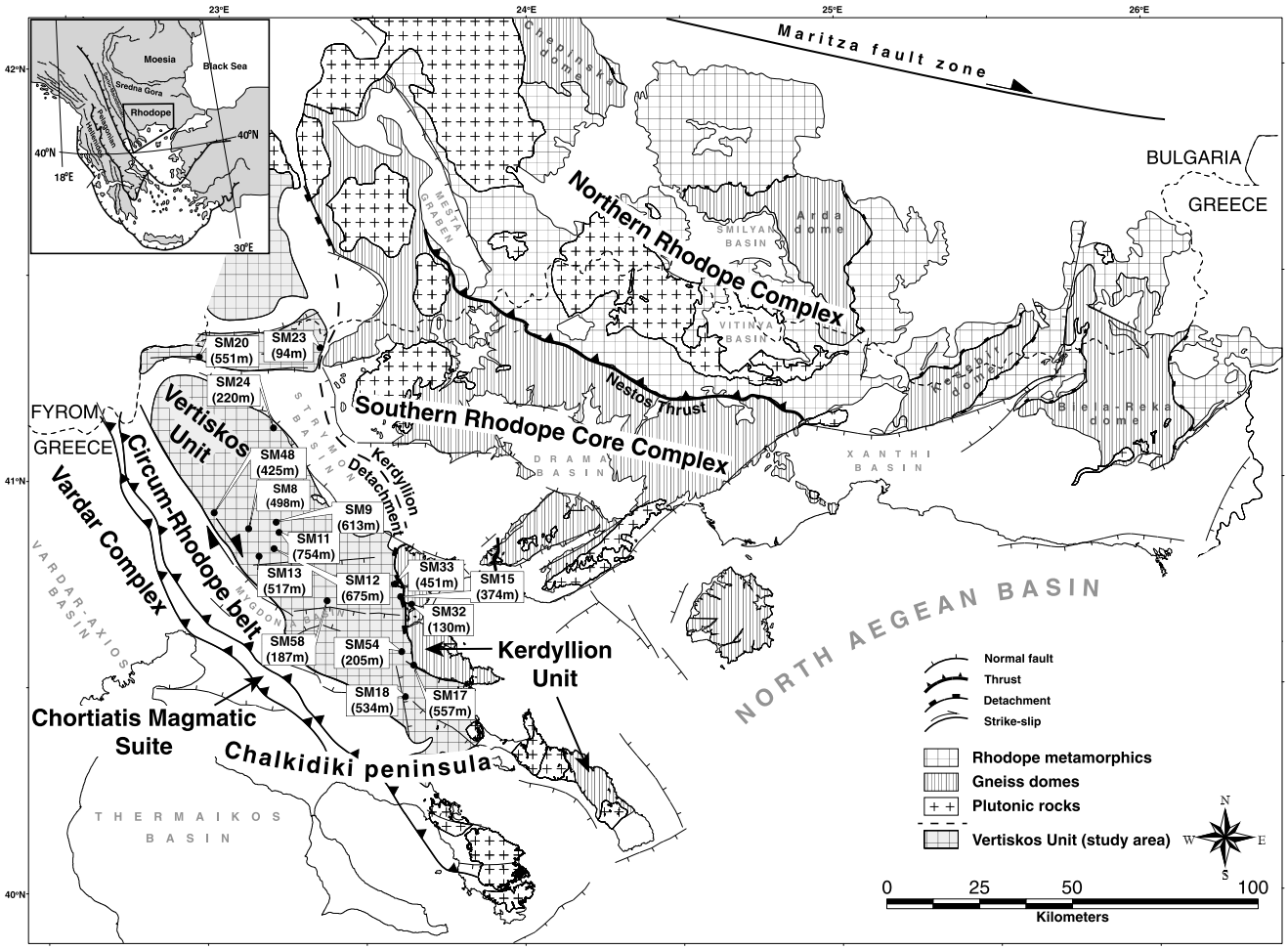

Figure 1. Simplified geological map of the Rhodope Metamorphic Province. Three tectonic domains can be distinguished, from northeast to southwest: (i) the Northern Rhodope Complex (NRC), (ii) the Southern Rhodope Core Complex (SRCC), and (iii) Serbo-Macedonian Domain (SMD). The latter is further subdivided into the lower Kerdyllion Unit, to the east, and the upper Vertiskos Unit (our study area) to the west. See text for details. Modified after *Kockel and Mollat* [1977], *Sakellariou and Dürr* [1993], and *Burg* [2012]. Normal faults after *Sokoutis et al.* [1993], *Tranos et al.* [2003], *Papanikolaou et al.* [2006], and *Brun and Sokoutis* [2007]. Our sampling locations (sample code and elevation) from the Serbo-Macedonian Domain are also shown.

2005] thus determining their low-temperature cooling path after the peak thermal event. This, combined with other low-temperature ([U-Th]/He) or mid-temperature ($^{40}Ar/^{39}Ar$) methods, can be used to decipher the regional signal of exhumation and cooling of an area.

In the present work we deal with the timing of regional cooling of the Serbo-Macedonian Domain and in particular its upper part namely the Vertiskos Formation (in the sense of *Kockel et al.* [1977]; Vertiskos Unit hereafter). For this purpose, new apatite FT age data and inverse thermal modeling for basement rocks are presented. We then proceed with comparing the obtained results with those from the central and eastern parts of the Rhodope Metamorphic Province summarizing also the available low-temperature data. This allows us to define first-order similarities and differences between different areas in terms of their low-temperature evolution during Upper Cretaceous-Tertiary.

2. Geological Setting

The Hellenides constitute an integral part of the Alpine-Himalayan mountain chain and are the product of convergence between the stable South European margin to the north and the North Gondwanan passive margin to the south. Their Alpine geodynamic evolution has been discussed at length by *van Hinsbergen et al.* [2005], *Jolivet and Brun* [2010], *Ring et al.* [2010], *Royden and Papanikolaou* [2011], and *Papanikolaou* [2013]. The centerpiece of the above studies is the continuous southward retreat of the subducting Hellenic slab

©2014. American Geophysical Union. All Rights Reserved.

since the Eocene that brought about a concomitant southward migration of magmatism in the severely extending Aegean lithosphere (upper plate), a slowdown in the rate of plate convergence coeval with acceleration of the trench retreat as well as a southward shift in the ages of progressively younger subduction-related metamorphism.

The Rhodope Metamorphic Province (RMP) [*Burg et al*., 1990; *Bonev et al*., 2006; *Krenn et al*., 2010; *Jahn-Awe et al*., 2010; *Nagel et al*., 2011] constitutes the hinterland of the Hellenic Subduction System (northeast Greece to southwest Bulgaria) (Figure 1). It can be viewed as a southwestward piling-up, crustal-scale, synmetamorphic, amphibolite-facies duplex [*Burg et al*., 1996; *Ricou et al*., 1998] strongly affected by later extension of core complex-type [*Sokoutis et al*., 1993; *Dinter and Royden*, 1993; *Brun and Sokoutis*, 2007] and syntectonic to posttectonic magmatism [e.g., *Kolocotroni and Dixon*, 1991; *Jones et al*., 1992; *Marchev et al*., 2004, 2013]. It is bordered to the north and east by the Maritza dextral strike-slip fault and the middle Eocene-present Thrace Basin, respectively. Its southwestern limit corresponds to the Vardar-Axios-Thermaikos basins which in turn roughly correlate with the Vardar Suture Zone (VSZ) [*Ricou et al*., 1998]. The continuity of the RMP to the south is hidden beneath the North Aegean Basin deposits [*Papanikolaou et al*., 2006]. In order to discuss the Upper Cretaceous-Tertiary thermal evolution of the area, we adopt a simple threefold division where the RMP is divided, from northeast to southwest, into three tectonic domains: (i) the Northern Rhodope Complex (NRC), (ii) the Southern Rhodope Core Complex (SRCC), and (iii) Serbo-Macedonian Domain (SMD; Figure 1).

The NRC (Figure 1) is characterized by a lithological variability reflecting the diversity of its constituting crustal fragments. Several units can be identified in the Greek and Bulgarian literature, all sharing a common Mesozoic-Cenozoic tectonometamorphic history [see *Burg*, 2012, and references therein]. The NRC is mainly made of orthogneisses, eclogites, and amphibolites, overlain by paragneisses, schists, and scarce marble horizons [*Mposkos and Liati*, 1993; *Liati and Seidel*, 1996; *Turpaud and Reischmann*, 2010; *Janák et al*., 2011; *Moulas et al*., 2013]. Volumetrically low ultramafic rocks also occur usually at high structural levels. Microdiamonds reported from gneisses of the NRC sets the RMP as the youngest diamondiferous ultrahigh pressure belt [*Mposkos and Kostopoulos*, 2001; *Perraki et al*., 2006; *Schmidt et al*., 2010] with pre-Upper Jurassic peak metamorphism [*Reischmann and Kostopoulos*, 2002; *Hoinkes et al*., 2008; *Nagel et al*., 2011; *Liati et al*., 2011, and references therein] and subsequent Cretaceous upper amphibolite-facies regional overprint [*Reischmann and Kostopoulos*, 2002; *Bauer et al*., 2007; *Bosse et al*., 2010; *Krenn et al*., 2010; *Liati et al*., 2011]. Basin deposits, unconformably overlying the exhumed metamorphic rocks, are dated as early as Maastrichtian-Paleocene [*Boyanov et al*., 1982; *Goranov and Atanasov*, 1992] and are related to plutonic rocks and volcanics of uppermost Cretaceous to lowermost Oligocene age [e.g., *Peytcheva et al*., 1998; *Soldatos et al*., 2001, 2008; *Ovtcharova et al*., 2003; *Marchev et al*., 2006, 2010; *Jahn-Awe et al*., 2010; *Filipov and Marchev*, 2011]. The deposits mark the initiation of extension affecting the nappe complex [see *Burchfiel et al*., 2000]. Distinct extensional gneiss domes exposed below low-angle detachments formed in late Eocene (Chepinska, Arda, Kesebir, and Biela-Reka domes; Figure 1) [see *Bonev et al*., 2006, 2013a; *Jahn-Awe et al*., 2012; *Kaiser-Rohrmeier et al*., 2013].

The SRCC (in the sense of *Brun and Sokoutis* [2007]) is a wide metamorphic dome of roughly triangular shape which lies immediately southwest of the NRC (Figure 1). Their contact is located along a mylonite-bearing SW verging thrust fault known as the Nestos Thrust. The SRCC consists of highly deformed Permian-Carboniferous mylonitic orthogneisses, intercalated mica-schists, and amphibolites capped by a thick marble sequence. The exhumed dome shows a flat-lying foliation over its width [*Brun and Sokoutis*, 2007]. The gneisses experienced upper greenschist to lower amphibolite-facies conditions, and the available metamorphic ages are exclusively post-Lower Eocene (post-51 Ma) [*Wawrzenitz and Krohe*, 1998; *Lips et al*., 2000]. Oligo-Miocene plutonic bodies that show syntectonic features intrude the basement rocks [*Kolocotroni and Dixon*, 1991; *Kaufman*, 1995; *Dinter et al*., 1995; *Eleftheriadis et al*., 2001]. Widespread NW-SE trending basins have developed after middle Miocene (e.g., Strymon and Drama basins; Figure 1) [*Snel et al*., 2006; *Burchfiel et al*., 2008] although remnants of mid-Eocene nummulite-bearing transgressive limestones have been reported locally (e.g., Xanthi basin).

The SRCC is bounded immediately to the west by the Serbo-Macedonian Domain (SMD; equivalent to "Serbo-Macedonian Massif" in the sense of *Dimitrijevic* [1963]) (Figure 1). The SMD can be traced from the Hellenic territory (Chalkidiki peninsula) [see *Kockel et al*., 1971] until Serbia to the far north. In the Hellenic domain, *Kockel et al*. [1971] divided the SMD into the lower Kerdyllion Unit and the upper Vertiskos Unit

©2014. American Geophysical Union. All Rights Reserved.

(Figure 1). *Himmerkus et al*. [2012] demonstrated the Rhodopean affinity of the lower Kerdyllion Unit. *Brun and Sokoutis* [2007] reinterpreted the contact between the Vertiskos and Kerdyllion Units as an extensional detachment fault, namely, the Kerdylion Detachment, that accommodated the exhumation of the SRCC since middle Eocene (Figure 1).

The Vertiskos Unit is an isolated and elongated basement belt with a pretty much constant width of approximately 30 km. In Bulgaria, to the north, it is known as the Ograzden Unit [*Zagorchev*, 1976]. In Greece, typical rock types are Silurian granitoids [*Himmerkus et al*., 2009a], later transformed into orthogneisses, intercalated paragneisses, and thin marble horizons, leucocratic granitic/pegmatitic intrusions, deformed amphibolites, and scarce eclogite boudins [*Kockel et al*., 1971, 1977]. The Vertiskos Unit was intruded in Lower Triassic by the Arnea-Kerkini magmatic complex [*Himmerkus et al*., 2009b] with which it experienced the same post-intrusion medium pressure amphibolite-facies overprint [*Burg et al*., 1995; *Kilias et al*., 1999]. The Permo-Triassic Volvi metamafic body crops out near the eastern part of the Vertiskos Unit and shows rift-related isotopic signature [*Bonev and Dilek*, 2010]. Similar to the NRC to the northeast where scarce uppermost Jurassic ages ($^{40}Ar/^{39}Ar$ on micas) have been reported in the literature for allochthonous orthogneisses (~155 Ma; Ku-214 and Ku-215 of *Bonev et al*. [2010]), *Lips et al*. [2000] reported a circa 147 Ma age for the Vertiskos Unit of Greece. In addition, *Kounov et al*. [2010] reported a circa 160 Ma age for the last six high-temperature gas release steps (white mica) from the equivalent Ograzden Unit of Bulgaria. Lower Cretaceous medium-temperature metamorphic ages are also abundant (circa 100–140 Ma for K/Ar and circa 80–160 Ma for Rb/Sr) [*Harre et al*., 1968; *Zervas*, 1979; *Papadopoulos and Kilias*, 1985; *de Wet et al*., 1989]. The structural continuity and the NW-SE trending fabrics of the Vertiskos Unit are disrupted by small sedimentary basins developed only after middle Miocene [*Koufos et al*., 1995]. Large Eocene batholiths [*de Wet et al*., 1989; *Christofides et al*., 1990] and limited Oligo-Miocene plutonic rocks [*Frei*, 1992; *Gilg and Frei*, 1994], often accompanied by small coeval volcanic extrusions [*Tompouloglou*, 1981; *Harkovska et al*., 2010; and our own data] intrude the Vertiskos Unit.

In summary, the Mesozoic-Cenozoic history of the three tectonic domains of the RMP is rather contrasted. The NRC is characterized by Jurassic-Cretaceous eclogite- and amphibolite-facies overprint, Maastrichtian basin deposits, Upper Cretaceous to Miocene magmatism, and Eocene migmatization within the exhumed gneiss domes. The SRCC is characterized by post-lower Eocene metamorphic ages, middle Miocene basin formation and Oligo-Miocene magmatism. The Vertiskos Unit records uppermost Jurassic to Lower Cretaceous metamorphic ages, middle Miocene basin formation and Eocene-Miocene magmatism.

3. Sampling Strategy

As mentioned above, there is clear evidence for Lower Cretaceous recrystallization at medium pressure amphibolite-facies conditions in the Vertiskos Unit. Initial exhumation of the unit can be considered as starting in the Upper Cretaceous based on zircon FT ages (71.9 ± 9.4 Ma in northern Greece by *Wuthrich* [2009] and 87.7 ± 8.6 Ma in southwestern Bulgaria by *Kounov et al*. [2010]). In Greece, close-to-surface exposure of the metamorphics is roughly constrained by a 43 ± 6.8 Ma apatite FT age [*Wuthrich*, 2009]. Therefore, a widespread cooling phase during Upper Cretaceous-Eocene seems to be recorded in the Vertiskos-Ograzden Units. However, the regional post-Lower Cretaceous cooling history and any possible lateral variations are yet to be investigated.

Here we focus on the Vertiskos Unit (Chalkidiki peninsula, northern Greece) with 15 samples: four orthogneisses, three granites, seven paragneisses, and one pegmatite (Figure 1 and Table 1). One additional sample from the underlying Kerdyllion Unit was analyzed. The lack of data in the studied area is in stark contrast with the wealth of published ages from the SRCC and the NRC to the east (see discussion below).

4. Apatite Fission Track Analysis

4.1. Analytical Methods

Apatite separation from the 16 samples was undertaken at Géosciences Rennes, France, following the procedure described by *Jolivet et al*. [2010]. The samples were crushed, and the apatite grains were separated using a Wilfley table, heavy liquids, and a Frantz isodynamic separator before being mounted on glass slides using epoxy resin and polished to expose an internal surface. We used the external detector method to calculate the

©2014. American Geophysical Union. All Rights Reserved.

Table 1. Fission Track Analysis[a]

Sample	Rock Type	Latitude	Longitude	Elevation	Number of Grains	$\rho_d \times 10^5$ (cm^{-2})	$\rho_s \times 10^5$ (cm^{-2})	$\rho_i \times 10^5$ (cm^{-2})	U (ppm)	P (χ^2)	Age (Ma)	±2σ	MTL	SD	Dpar
SM8	O	40.90	23.12	498	40	9.375 (9,098)	20.148 (2,182)	55.928 (6,057)	68	73	57.0	1.9	12.99	1.17	1.17
SM9	G	40.91	23.21	613	40	9.651 (9,098)	7.246 (1,321)	24.279 (4,426)	32	84	48.7	1.9	13.10	1.52	1.48
SM11	P	40.88	23.22	754	40	9.992 (10,419)	5.325 (639)	15.558 (1,867)	20	63	57.7	3.0	13.18	1.03	1.36
SM12	O	40.84	23.21	675	33	10.087 (10,419)	6.876 (647)	23.039 (2,168)	27	100	50.8	2.5	13.51	0.90	0.99
SM13	P	40.83	23.16	517	40	10.372(10,419)	5.791 (911)	18.086 (2,845)	20	97	56.1	2.5	13.05	1.14	1.04
SM15	P	40.73	23.61	374	26	10.656 (10,419)	4.549 (348)	15.32 (1,172)	16	92	53.4	3.5	-	-	-
SM17	P	40.57	23.66	557	37	10.846 (10,419)	3.263 (218)	11.063 (739)	12	100	54.0	4.3	-	-	-
SM18	P	40.49	23.62	534	28	9.433 (10,362)	3.464 (239)	11.855 (818)	14	99	46.6	3.6	-	-	-
SM20	O	41.31	22.93	551	26	9.94 (10,362)	2.979 (188)	9.239 (583)	11	92	54.1	4.7	-	-	-
SM23	O	41.34	23.33	94	36	10.431 (10,905)	7.599 (785)	27.957 (2888)	30	90	47.9	2.2	13.51	1.06	1.24
SM24	P	41.13	23.21	220	26	10.278 (10,362)	4.368 (280)	15.226 (976)	16	48	50.1	3.7	-	-	-
SM32	P	40.71	23.65	130	28	10.16 (10,905)	2.449 (226)	9.491 (876)	11	99	44.3	3.4	-	-	-
SM33	G	40.76	23.58	451	33	9.889 (10,905)	12.618 (1,147)	40.814 (3,710)	47	59	51.6	2.1	13.54	1.24	2.12
SM48	PE	40.93	23.01	425	33	10.615 (10,362)	8.315 (528)	21.732 (1,380)	23	97	68.5	3.8	13.31	0.93	1.13
SM54	P	40.61	23.60	205	18	10.784 (10,362)	1.156 (52)	2.4 (108)	3	100	87.4	14.9	-	-	-
SM58	G	40.72	23.38	187	20	11.122 (10,362)	1.912 (108)	6.372 (360)	7	95	56.3	6.3	13.26	1.28	-

[a]All samples are from the Vertiskos Unit with the exception of SM32 which belongs to the Kerdyllion Unit. Rock type: (O) orthogneiss, (G) granite, (P) paragneiss, (Pe) pegmatite. Latitude/longitude is given in WGS1984. ρ_d is the density of induced fissions tracks (per cm^2) that would be obtained in each sample if its U concentration was equal to the U concentration of the CN5 glass dosimeter. Numbers in parentheses are total number of tracks counted. ρ_s and ρ_i are the sample spontaneous and induced track densities per cm^2. U is the calculated uranium concentration in ppm. P(χ^2) is the probability in % of χ^2 for ν degrees of freedom (where ν = number of crystals −1). Age is central age, according to *Galbraith and Laslett* [1993], given in Ma and calculated using the TRACKKEY software [*Dunkl*, 2002]. Error is given at ±2σ. Mean track length (MTL) is given in μm, and measurements were performed on horizontal confined fission tracks in crystal sections parallel to the *c* crystallographic axis. Dpar is the measured mean diameter (in μm) of the etched trace of the intersection of a fission track with the surface of the analyzed apatite crystal, measured parallel to the *c* axis.

FT ages [*Gleadow*, 1981; *Hurford and Green*, 1982]. The polished apatite mounts were etched in 6.5% HNO_3 (1.6 M) for 45 s at 20°C to reveal the spontaneous fission tracks, and a low-U external mica sheet was attached before being irradiated with a neutron fluence rate of 1.0×10^{16} neutrons/cm^2 (OSU, Oregon State University, USA). CN5 dosimeters were used to monitor the neutron flux [*Hurford and Green*, 1983]. The induced tracks in the external detector were etched with 60% HF for 40 min at 20°C.

The AFT age measurements were made at Géosciences Rennes with a Zeiss M1 microscope at 1250X magnification under dry objectives. For each sample between 18 and 40 *c* axis-oriented, inclusion-free apatite crystals were analyzed using the Trackscan® and TrackWorks® software packages in manual mode. Age calculations were made with the TrackKey® software [*Dunkl*, 2002] using a weighted mean ζ value equal to 339.1 ± 6.8 (K.K.) obtained on both Durango and Mount Dromedary apatite standards. All ages reported are central ages according to *Galbraith and Laslett* [1993]. Errors on ages are quoted at 2σ.

Length measurements of horizontal confined tracks and etch pit dimensions (as a proxy for apatite composition) [*Barbarand et al.*, 2003; *Carlson et al.*, 1999; *Ketcham et al.*, 2007] were made with a Zeiss Axioplan microscope (Birkbeck University of London) equipped with a digitizing tablet and computer-driven stage with 1250X magnification using dry objectives. Dpar measurements were calibrated against Durango standards (K.K.).

4.2. Results

The results of the AFT analysis are presented in Table 1 (see supporting information for the full data set). For each sample between 18 and 40 single grains were used for the age calculation (Figure S1). For the Vertiskos Unit, a tight cluster of apatite FT ages range from 46.6 ± 3.6 to 57.7 ± 3.0 Ma. The

©2014. American Geophysical Union. All Rights Reserved.

westernmost sample (SM48) is a deformed pegmatite which yielded a significantly older age (68.5 ± 3.8 Ma). SM54 gave an exceptionally old age of 87.4 ± 14.9 Ma but due to its poor grain quality (cracked crystals with plenty of inclusions), low uranium content (<3 ppm), wide range of individual grain ages (χ^2 value of 3.72), and the fact that this age does not fit the rest of the results, this sample will be excluded from further consideration. The apatite FT age from the Kerdyllion Unit is 44.3 ± 3.4 Ma (SM32), slightly younger than those of the Vertiskos Unit.

Track lengths and the corresponding *c* axis angle were obtained for nine samples of the Vertiskos Unit (Figure S2). Hundred individual lengths were measured for the majority of the samples with the exception of three samples (41, 81, and 86 length measurements for SM58, SM11, and SM9, respectively). The calculated mean track length (MTL) ranges from 13 to 13.5 μm and the standard deviations from 0.9 to 1.5 μm. Eight samples were used for Dpar measurement. An average of 220 measurements was made for each sample (made on 42–67 individual grains). With the exception of SM33 which shows high Dpar value (2.12 μm), the rest of the samples range from 0.99 to 1.48 μm indicating F-rich apatites.

5. Inverse Thermal History Modeling

5.1. Methodology

Given the fission track analysis for a given sample, we can infer the thermal history of each sample individually using an inverse modeling scheme. Here we adopted the Markov Chain Monte Carlo (MCMC) approach described by *Gallagher* [2012], implemented in the software QTQt. Details of the specific implementation can be found in *Gallagher* [2012] and other implementations of MCMC can be found in *Gallagher et al*. [2009], *Charvin et al*. [2009], *Hopcroft et al*. [2007], and *Sambridge et al*. [2006]. In brief, the applied inversion scheme is based on Bayesian transdimensional sampling in which the complexity of the thermal history solutions (defined as the number of discrete time-temperature points forming the thermal history) are inferred from the data rather than being specified in advance. The Bayesian approach naturally prefers simpler thermal history models and so reduces problems associated with over interpreting the data (i.e., introducing unwarranted structure in the inferred thermal histories). The output of the method is a population of thermal histories, which reflects the range of acceptable models in terms of a (posterior) probability distribution. Individual models, such as the best data-fitting (maximum likelihood) model or the expected model (effectively the weighted mean thermal history from the posterior distribution) can be also extracted from the posterior distribution to visualize a single thermal history. Additionally, the QTQt implementation allows a group of individual samples of different elevations to be treated as a vertical profile (equivalent to a borehole in the upper crust). In this approach, we make the implicit assumption that all the samples have experienced a similar form of thermal history, with lower elevation samples having always been hotter or at least as hot as the higher-elevation samples and there have been no major disruptions of this geometrical/structural relationship since the samples cooled through the apatite fission track PAZ [*Gallagher et al*., 1998].

5.2. Results

As mentioned earlier, a wealth of available medium-temperature geochronology data exist in the literature for the basement rocks of the Vertiskos Unit. They include Ar/Ar, K/Ar, and Rb/Sr data from orthogneisses, biotite gneisses, intercalated pegmatites, and garnet-mica schists. The Ar/Ar system peaks at circa 150 Ma [*Lips et al*., 2000; *Kounov et al*., 2010]. The K/Ar system culminates at Lower Cretaceous (between 100 and 140 Ma) [*Harre et al*., 1968; *Marakis*, 1969; *Papadopoulos and Kilias*, 1985]. The Rb/Sr isochrons points variably between uppermost Jurassic and Upper Cretaceous times [*Zervas*, 1979; *Lilov et al*., 1983; *Papadopoulos and Kilias*, 1985; *de Wet et al*., 1989]. For this, we can safely conclude that the temperature remained high enough to cause complete annealing in the FT data at least until the end of Lower Cretaceous. To respect this independent geological evidence, we constrained the model histories to pass through 350 ± 50°C at 100–140 Ma. As this is well above the apatite partial annealing zone, there is no significant effect on the thermal history models inferred from the inverse modeling.

5.2.1. Individual Sample Inverse Modeling Results

We used the nine samples from the Vertiskos Unit for which length data were obtained (Table 1). At this stage we treat each sample individually and allow the Dpar (proxy for apatite composition) to vary within the variance obtained from the measurements). The results for the expected and maximum likelihood models as well as the predictions on the FT age, MTL, and the sampled values for Dpar are shown in Figure 2. A summary of the observed versus predicted/sampled values for the FT age, MTL, and Dpar is shown in Figure 3.

©2014. American Geophysical Union. All Rights Reserved.

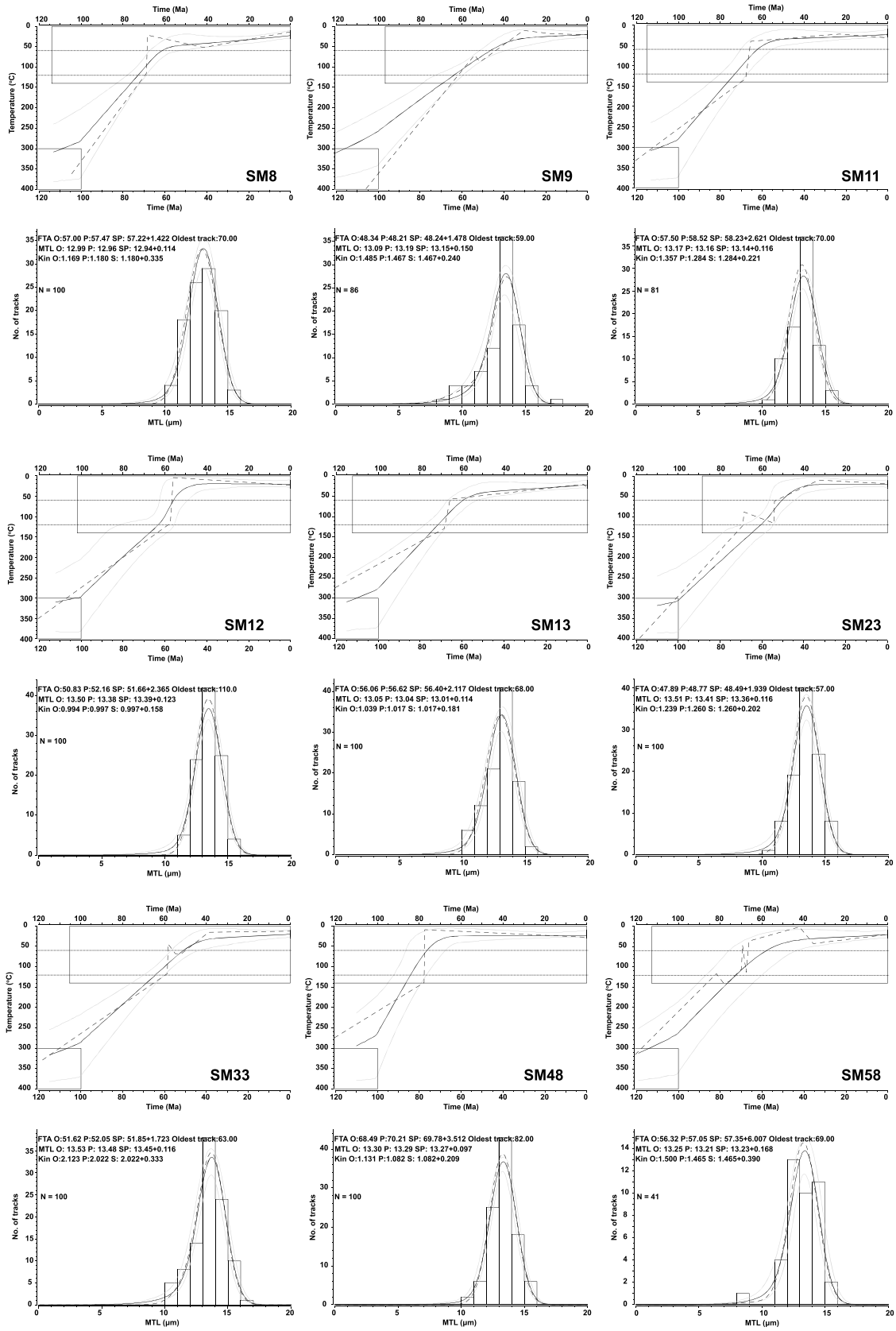

Figure 2

©2014. American Geophysical Union. All Rights Reserved.

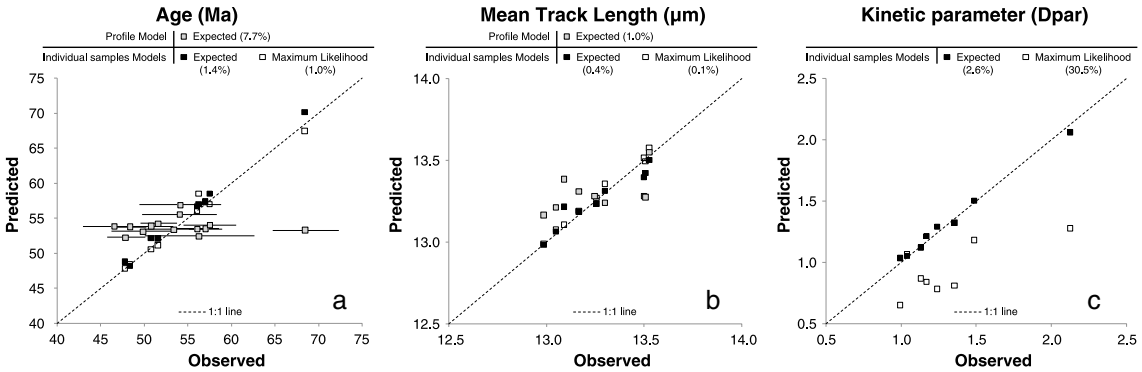

Figure 3. Observed versus predicted values of both the individual sample modeling (expected and maximum likelihood models) and the joint profile modeling approaches adopted here for (a) the age, (b) the mean track length, and (c) the sampled kinetic parameter. Error bars on the observed age are also shown for part of the data set. Numbers in parentheses is the average percentage deviation from the observed values for each data set.

The thermal history represented by the expected model tends to be simpler or smoother than the maximum likelihood model (Figure 2), although predictions using the latter will be closer to the measured data. As a result, the maximum likelihood model fits the AFT age and MTL data (Figures 3a and 3b) but not the sampled parameter Dpar (Figure 3c). The deviation from the observed values tends to be as low as 1% (average for both models) with the exception of the Dpar prediction for the maximum likelihood model (30% on average). The maximum likelihood model arrives at systematically lower mean Dpar than the measured values. However, as a test on the significance of the actual Dpar value on the inferred thermal history, we fixed its value to the observed one and reran the inversions. The results were not significantly different in terms of the timing of cooling episodes.

Overall, the thermal histories of the nine modeled samples are similar in that they all show one major period of cooling in the Upper Cretaceous. Figure 4 summarizes the results of inverse modeling (we show both the maximum likelihood and expected models). For the vast majority of the samples (SM48 excluded) the maximum likelihood models show rapid cooling through the apatite FT partial annealing zone roughly between 50 and 70 Ma without any reheating thereafter (Figure 4). SM48 shows the same general trend, but its rapid cooling phase is at 80 Ma; this is caused by its old FT age (68.5 ± 3.8 Ma). A more complicated history (more T-t points), yet the same general shape, is inferred for sample SM58 but this may be due to the fact that only 41 length measurements were obtained.

The expected models show the same general form but tend to be smoother than the maximum likelihood models (Figure 4). These average thermal histories show more or less linear cooling from the constrained T-t area to close-to-surface temperature (below 50°C). Eight out of the nine modeled samples (SM48 excluded) form a cluster and their thermal history crosses the high-temperature limit of the apatite partial annealing zone (~120°C) between circa 55 and 75 Ma, ~5 Myr later than the rapid cooling shown by the maximum likelihood models. This reflects the level of uncertainty on the timing of cooling for all the thermal histories accepted by the MCMC sampling. Sample SM48 crosses the same temperature boundary at 84 Ma. All samples are at temperature lower than 50°C since 45 Ma at the latest.

In Figure 5, all the samples are plotted along a WSW-ESE transect over a swath profile covering the width of the Vertiskos Unit (sampling area). There is potentially a geographical trend for younger ages toward the east (SM54 excluded). However, if the uncertainty on the age calculation is considered, this trend becomes less obvious and the ages of adjacent samples often overlap within error. Considering the inferred thermal histories for the expected model in more detail, they show the same general form but from the westernmost sample (SM48) to the easternmost ones (SM23 and SM33), the thermal paths enter the PAZ at younger times

Figure 2. Summary of model results and predictions for nine samples from the Vertiskos Unit (see Figure 1 for sample location). For each sample the upper graph shows the inferred thermal history for the expected model (solid black line with 95% credible interval range represented by grey solid lines) and the maximum likelihood model (dashed line). The lower graph shows the predicted and observed length distributions, for the expected model in black line with 95% credible interval range represented by grey solid lines and for the maximum likelihood model in dashed line. See *Gallagher* [2012] for details of the modeling procedure adopted here.

©2014. American Geophysical Union. All Rights Reserved.

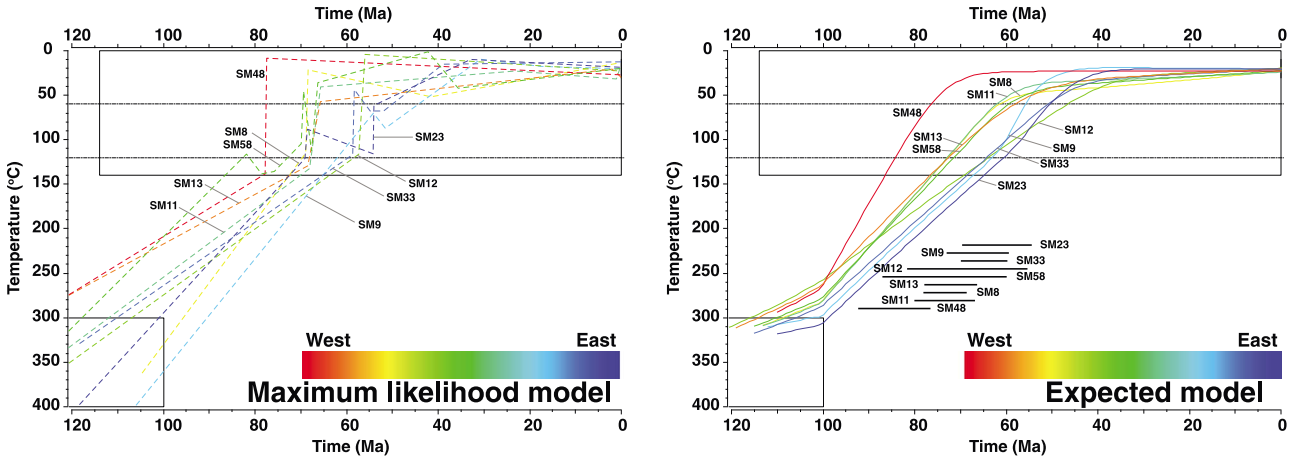

Figure 4. Compilation of the calculated (left) maximum likelihood and (right) expected models for nine samples of the Vertiskos Unit that inferred using the individual samples approach (shown also in Figure 2). See Figure 1 for sample locations. For the expected model (right), the timing (2 sigma uncertainty included) that each individual thermal path (sample) crosses the high-temperature boundary of the apatite PAZ (~120°C) is also indicated.

following the geographic trend mentioned above (Figure 4). However, this intriguing geographical pattern needs to be considered in the context of the uncertainties on the thermal histories. Plotting the uncertainties (2 sigma) on the timing that each thermal path crosses the high-temperature boundary of the PAZ (~120°C), significant overlap exists for all, but SM48, samples (black horizontal lines; Figure 4). This suggests that the apparent geographical trend is either not real and/or the AFT data are not sensitive enough to record unambiguously such variation especially taking into consideration the relatively narrow width (~30 km) of the studied area (Figure 1).

Irrespective of the details of the individual thermal histories, the overall picture extracted from modeling each sample independently implies that the basement rocks of the Vertiskos Unit cooled through the apatite PAZ between the uppermost Cretaceous and the lower/middle Eocene.

5.2.2. Profile Modeling Results

Having modeled the thermal history for each sample independently, we now consider them as representing a vertical profile. The aim of this is to determine whether we can explain the data from all samples with a simple and common thermal history to assess whether the geographical variation in the thermal histories described above is real. In this approach, we model all samples simultaneously, using the present-day elevation differences as a proxy for different depth in the crust during cooling [*Gallagher et al*., 2005a, 2005b; *Stephenson et al*., 2006]. As shown by *Gallagher et al*. [2005a], this joint modeling approach minimizes artifacts in the resulting thermal histories (such as the reheating events in Figure 4 for some of the maximum likelihood solutions). The differences in elevation are then used to estimate the temperature difference between the uppermost and lowermost samples, and the thermal histories for samples between them are calculated using linear interpolation of this temperature offset. All the samples are considered to have experienced the same form of thermal history and the reasonable assumption is that the lowest elevation

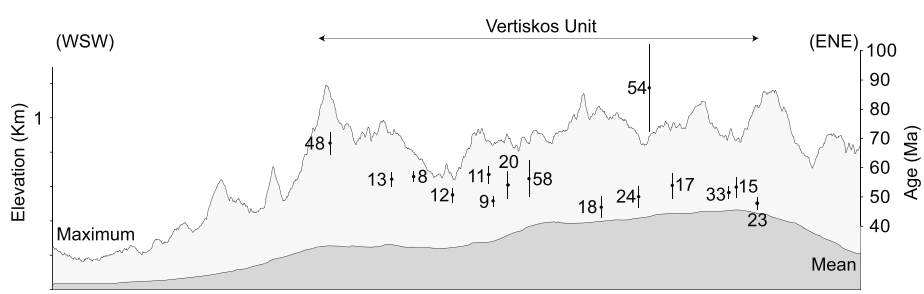

Figure 5. WSW-ENE trending swath elevation profile of the Chalkidiki Peninsula extracted from the ASTER Global DEM v2. The profile stretches from the Vardar-Axios basin to the Strymon basin (see Figure 1). The AFT ages for the samples used for the joint profile modeling approach are plotted, and the corresponding calculated apatite FT ages are read on the right vertical axis.

©2014. American Geophysical Union. All Rights Reserved.

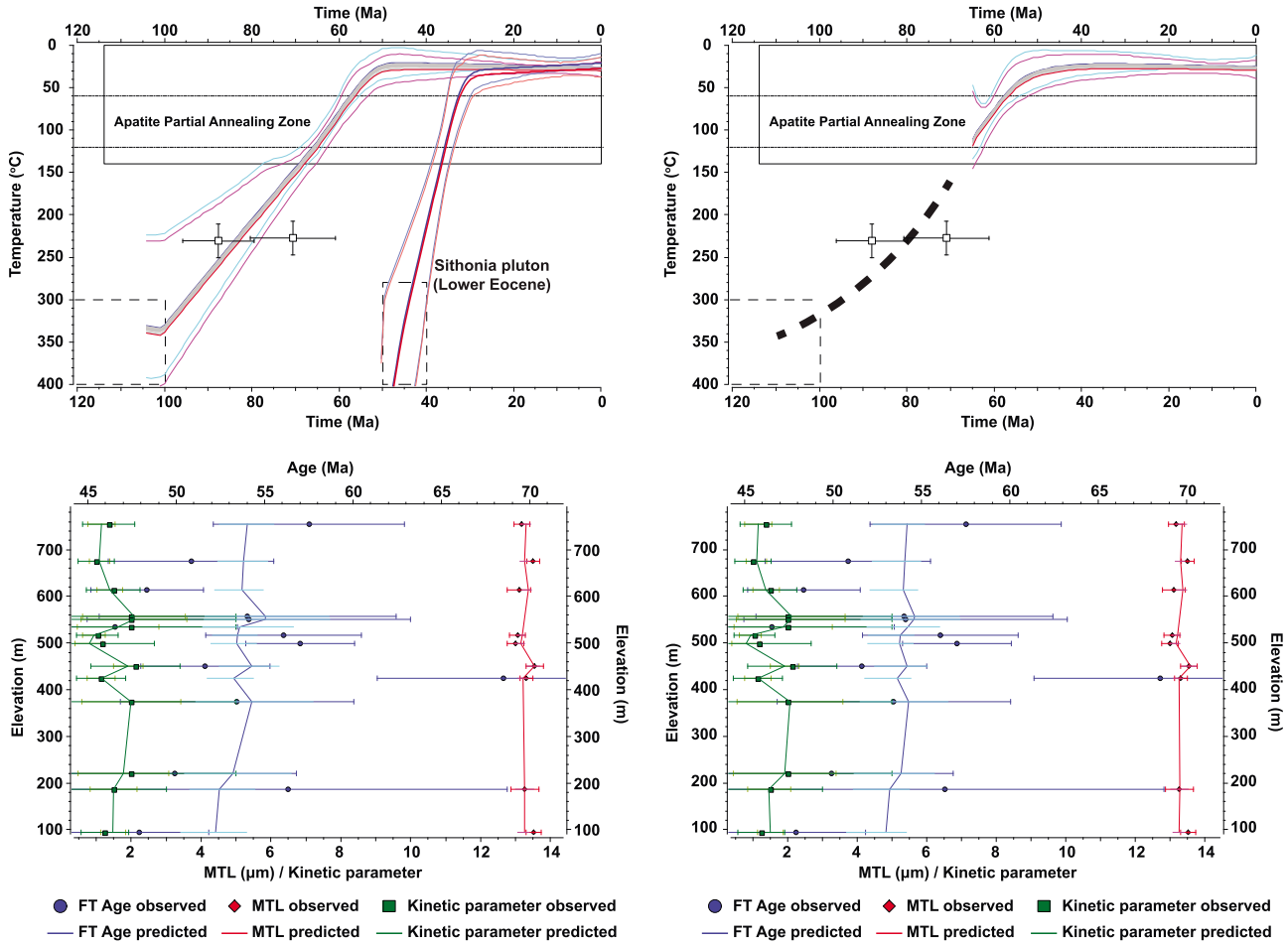

Figure 6. (top) The inferred expected model for 14 basement samples of the Vertiskos Unit treated as a vertical profile. The samples used are also shown in Figure 5 (SM54 excluded). The modeling approach is described in *Gallagher et al.* [2005b] and *Gallagher* [2012]. The model on the left originates from a constrained T-t area (dashed box; 350 ± 50°C at 120 ± 20 Ma) based on the geological evidence and the available geochronology data (see text for details). The two empty squares correspond to the published ZFT age from the Vertiskos/Ograzden Units. For comparison, the result of the nonconstrained model is shown on the right. Red thick line is used for the thermal path of the hottest (lowest-elevation) sample (red thin lines 95% credible interval range) and blue thick line for the thermal path of the coolest (highest-elevation) sample (blue thin lines 95% credible interval range). Using the same modeling approach and the samples GR117, GR126, GR132, and GR134 from *Hejl et al.* [2010], we calculated, for comparison, the thermal path of the lower Eocene Sithonia pluton from the southern edge of the Chalkidiki peninsula (see Figure 1 for location). (bottom) The corresponding FT age (blue), mean track length (red), and kinetic parameter (green) predictions for the constrained and nonconstrained models are shown.

samples were always hotter (deeper in the crust prior to exhumation) than their highest-elevation counterparts which remained shallower in the crust. Under these assumptions, we can extract the regional thermal history of the sampled area. In such an approach we exploit the spatial link between different samples in the vertical sense. This includes the implicit assumption that any syncooling or postcooling vertical displacement (e.g., faulting) between sampling locations is negligible. As seen in Figure 1, there is no basin of significant size fragmenting the Vertiskos Unit. One exception is the relatively small middle Miocene Mygdonia basin which is known to be quite shallow (not exceeding 200 m) [*Koufos et al.*, 1995].

Given the assumptions above, this approach allows us to (i) integrate samples with no track length measurements with those that do have them, (ii) to minimize the complexity of the inferred thermal histories of individual samples (previous section), and (iii) to illustrate the thermal evolution of the study area as a whole, grouping the individual samples. Comparing the thermal histories obtained by modeling all samples together to those obtained by modeling them individually, we can heuristically assess the validity of the approach and the assumptions above.

We used 14 of the basement samples from the Vertiskos Unit (Table 1; SM54 excluded). All of the samples contain age data, and nine of them have both age and FT length data. The measured central ages range

©2014. American Geophysical Union. All Rights Reserved.

between 46.6 ± 3.6 Ma and 68.5 ± 3.8 Ma and the elevation range from 94 m to 754 m. The resultant thermal history is relatively simple (Figure 6) and similar in form to those inferred for each sample individually (Figure 4). For comparison, the nonconstrained profile model is also shown in Figure 6. The inferred thermal history shows linear type of cooling between the constrained T-t area and the near-surface conditions. The cooling path crosses the high-temperature limit of the apatite FT partial annealing zone between 62 and 70 Ma (uncertainties included), and it stays at temperature below 50°C since 55 Ma. The inferred temperature difference between the highest- and the lowest-elevation samples is 9 ± 7°C (1 sigma), which implies that the data do not necessarily require very different thermal histories. Although we have grouped together a suite of samples spread over a relatively large area to search for a common form of the thermal history, the data fit is still acceptable in terms of predicted versus observed age and the same for the MTL and sampling of the kinetic parameter (Figures 3 and 6). Only 3 out of the 14 samples did not have predicted ages within error, while all of the predicted/sampled values for MTL and Dpar were within error of the observed values.

6. Discussion

6.1. Comparing the Two Modeling Approaches

We have used here AFT analysis and two inverse modeling approaches to investigate the post-Lower Cretaceous cooling path of the Vertiskos Unit (Figure 1). In the first approach we modeled each sample independently allowing, thus, for different solutions for each sample (Figure 4). In the second approach, we modeled all samples together assuming that they represent a vertical profile and restricting the possible solutions to one common (and simple) thermal history (Figure 6). As expected, the first approach resulted in better data fit than the second one (Figure 3) [see also *Gallagher et al*., 2005a, 2005b].

From the swath profile shown in Figure 5, a possible eastward younging of the ages can be inferred. This trend becomes ambiguous when considered in the context of the age uncertainties (overlapping ages within error). Using the first approach (individual sample modeling), the same trend is reflected in the resulting thermal histories which also tend to show a later (younger) cooling into the PAZ toward the east (Figure 4). Using the second approach (joint profile modeling) under assumptions mentioned earlier (see sections 5.1 and 5.2.2), a similar (in form and timings) thermal history is inferred from the data (Figure 6). In this case, the FT age for the westernmost sample (SM48), which gives the earliest cooling through the PAZ (around 80–85 Ma) is not so well predicted by the joint profile thermal histories (Figure 6), suggesting that this sample is not consistent with the profile-modeling assumptions. However, the similarity in the form and spread of the individual expected thermal histories (Figure 4), and the profile thermal histories (with their uncertainties shown in Figure 6) for the other samples suggests either that overall the assumptions are valid or that the data are not sensitive enough to answer which of the two modeling approaches is better for the case of the Vertiskos Unit. To resolve that and to assess whether the geographical variation in the AFT ages (Figure 5) is real, a more dense sampling grid coupled with both lower ([U-Th]/He) and higher temperature methods (Ar/Ar on potassic feldspars, ZFT) would be necessary.

Overall however, the results of the two approaches are not significantly different in terms of form of the cooling path and timing. Considering the Vertiskos Unit and independently of the chosen modeling approach, the outcome of our AFT analysis is that it remained at temperature of approximately 120°C until uppermost Cretaceous, and it was at near-surface temperature (less than 50°C) by lower/middle Eocene (Figures 4 and 6). With the current state of knowledge and available data and in the absence of any conclusive evidence, both approaches will be discussed independently in the following sections and a possible mechanism for explaining the geographical variation, treated in the first approach, will be presented.

6.2. Regional Geological and Thermal Evolution of the Vertiskos Unit

The Vertiskos Unit of the Chalkidiki peninsula, northern Greece, is a complex unit with a poly-metamorphic history (Figure 1). Its pre-Jurassic history can be described in terms of a coherent metamorphic fragment that detached from the northern Gondwanan margin and was incorporated into the Variscan Arc of southern Europe during the Carboniferous [*Kydonakis et al*., 2014]. Equivalent units can now be traced to Bulgaria and to Serbia farther north [see *Zagorchev*, 1976; *Dimitrijevic*, 1963; see also *Kounov et al*., 2010, 2012]. In Greece it mainly comprises Silurian granitoids, later transformed into orthogneisses, intercalated garnet-mica schists, amphibolites, and thin marble horizons [*Himmerkus et al*., 2006, 2009a; see also *Kockel et al*., 1971, 1977]. In Bulgaria, the protolith age of equivalent orthogneisses (Ograzden Unit) is defined as Ordovician [*Zidarov et al*., 2003; *Macheva et al*., 2006; see also *Bonev et al*., 2013b]. An extensive rifting event dispersed the arc

©2014. American Geophysical Union. All Rights Reserved.

systems of southern Europe during the Triassic and caused the opening of oceanic basins. In northern Greece, the Vertiskos Unit represents such a rifted part of the European Arc systems, south of which the Vardar Oceanic Domain opened. The rifting event is clearly documented by widespread Triassic granitic intrusions known collectively as the Arnea-Kerkini Complexes [*de Wet et al*., 1989; *Himmerkus et al*., 2009b; *Poli et al*., 2009] and the related Volvi metamafic body [*Himmerkus et al*., 2005; *Bonev and Dilek*, 2010; *Liati et al*., 2011].

During the Alpine Orogeny and the closure of the Vardar Ocean, the Vertiskos Unit was incorporated into the southern European active margin reaching lower amphibolite-facies conditions (garnet-staurolite degree). Based on the available medium temperature geochronological data for the basement rocks of the Vertiskos Unit, the temperature remained high enough to reset the K/Ar (and partly the Rb/Sr) system during the Lower Cretaceous [*Harre et al*., 1968; *Zervas*, 1979; *Papadopoulos and Kilias*, 1985; *de Wet et al*., 1989]. In the southern tip of the Chalkidiki peninsula a first pulse of magmatic intrusions is recorded (Figure 1). Hornblende-biotite granodiorites (Sithonia, Ierissos, Ouranoupolis, and Gregoriou), dated at circa 50 Ma [*de Wet et al*., 1989; *Christofides et al*., 1990; *Frei*, 1996], intruded the basement complex. Their continuation to the south is obscured by the sea, while to the north, along the Vertiskos Unit, no magmatism of the same age is recorded. They belong to an extensive magmatic pulse that is recorded further to the northeast in the NRC (see below). Within the Vertiskos Unit, a second pulse of magmatic activity is documented by smaller plutons (Stratoni, Skouries, and Olympiada) that are often accompanied by volcanic extrusions (Monolithi and Gerakario). Feeding dykes of the latter intrude the basement complex marking the time of its final surface exposure. To the south they are related to fluid circulation, porphyry copper mineralization, and Pb-Zn-Ag-Au replacement ores. This pulse is as old as Oligo-Miocene [*Frei*, 1992; *Gilg and Frei*, 1994; *Tompouloglou*, 1981; and our own data]. It can be traced at least up to southwest Bulgaria (Kozhuh volcanic body) [*Pecskay et al*., 2011] where it intrudes the equivalent Ograzden Unit.

The post-Lower Cretaceous cooling of the Vertiskos Unit as a coherent block can be inferred from the results of the vertical profile modeling (Figure 6). The cooling path crosses the high-temperature limit of the apatite FT partial annealing zone (~120°C) at uppermost Cretaceous (between 62 and 70 Ma) and remains at temperature $<$50°C since the lower Eocene. Using the available geochronology data [*Hejl et al*., 2010] for a typical Lower Eocene pluton of the first magmatic pulse (Sithonia pluton from the southern tip of the Chalkidiki peninsula; Figure 1) and the profile modeling technique described in a previous section, we can demonstrate that this pluton cooled to 50°C as early as lowermost Oligocene (~33 Ma), i.e., 10–15 Myr later than the surrounding basement rocks (Figure 6). Thus, it can be concluded that none of the two magmatic pulses penetrating the Vertiskos Unit (Eocene and Oligo-Miocene) were strong enough to cause regional thermal perturbations. Local thermal perturbations are possible, but, to first order, do not appear to be too significant, given the overall similarity of the profile and individual sample modeling results.

In summary, the Vertiskos Unit preserves evidence for Upper Cretaceous exhumation and lower/middle Eocene near-surface exposure documented by low-temperature thermochronology data. This robust and systematic low-temperature record over a distance of several tens of kilometers is a unique feature of the Rhodope Metamorphic Province. The regional exhumation of the Vertiskos Unit clearly predates any basin formation and the two described thermal pulses caused by plutonic intrusions.

6.3. Lateral Variations of the Cooling Histories in the Vertiskos Unit

In order to evaluate the scale and significance of lateral variations in the cooling history of the Vertiskos Unit we return to the results of the individual sample modeling (Figure 4). Lateral variations in the measured apatite FT ages have already been discussed (see section 6.1); they young toward the east (Figure 5). This trend is clearly reflected into the corresponding individual thermal histories which also become younger toward the east (Figure 4). In other words, the relatively young unroofing of the eastern part of the Vertiskos Unit is in contrast to the earlier cooling recorded in its western part. Here we consider possible explanations for this variation.

The Vertiskos Unit is bordered along its western side by a pile of Mesozoic metasediments (known as the "Circum-Rhodope" belt) (in the sense of *Kauffmann et al*. [1976]) and a Jurassic magmatic arc (namely, the "Chortiatis Magmatic Suite") [see *Kockel et al*., 1971] via composite contacts showing thrust and dextral strike-slip components [*Ricou and Godfriaux*, 1994; *Tranos et al*., 1999] (Figure 1). The youngest involved sediments are virtually unmetamorphosed calcareous clastics of Albian-Cenomanian age [*Meinhold et al*.,

©2014. American Geophysical Union. All Rights Reserved.

2009]. This implies that thrusting was active at shallow crustal conditions during the Upper Cretaceous along the western border of the Vertiskos Unit. During the same time, we have shown evidence for exhumation of the Vertiskos Unit from midcrustal level to the surface (Figure 4). Assuming that differential erosion occurred, exhumation of its western shoulder through a thrusting mechanism would have resulted in younger ages toward the west. Therefore, this mechanism cannot explain the observed FT age and inferred thermal history variations.

Brun and Sokoutis [2007] described the Kerdyllion Detachment as the structure which controlled the exhumation of the SRCC from middle Eocene to middle Oligocene immediately east of the Vertiskos Unit (Figure 1). During that time, the Vertiskos Unit was the hanging wall of the detachment on top of the exhuming mylonitic gneisses. As illustrated in Figure 4, the Vertiskos Unit was already at shallow depth and at temperature less than 50°C before the formation of the SRCC. Therefore, any thermal disturbance related to the exhumation of the mylonitic gneisses and the syntectonic plutons postdates the exhumation of the Vertiskos Unit and can neither affect its thermal evolution nor explain the observed lateral variations in age or cooling through the PAZ. We argue that the observed geographical age geographical pattern can be explained with passive postexhumation asymmetric uplift and erosion of the eastern Vertiskos shoulder due to extensional doming of the SRCC immediately to the east (Figure 1). In such a way its deeper parts are exposed along the eastern side resulting to younger FT ages and later cooling through the PAZ (Figure 4). Indeed, the eastern side of the Vertiskos Unit stands at higher elevation compared to its western side, showing, overall, an asymmetric relief (Figure 5). The asymmetry decays toward the west, away from the exhuming SRCC, where the oldest ages are recorded. The same result can be also triggered by the middle Miocene, NW trending, NE dipping normal faults bordering the Strymon basin along the eastern part of the Vertiskos Unit (Figure 1). Exhumation along their footwall would expose deeper parts of the Vertiskos Unit.

In summary, the younger FT ages (and their associated thermal histories) toward the east within the Vertiskos Unit is arguably the result of postexhumation passive tilting essentially combined with increased erosion rates toward the east. The relatively young extensional exhumation of the SRCC immediately to the east of the Vertiskos Unit and/or the middle Miocene normal faulting along its eastern border both account for possible mechanisms.

6.4. Comparing the Vertiskos Unit to the Rhodope Metamorphic Province

The Rhodope Metamorphic Province is made of three main tectonic domains that display first-order similarities and differences in terms of cooling to near-surface temperature (Figure 7). The available low-temperature thermochronology data [from *Bigazzi et al*., 1994; *Kyriakopoulos et al*., 1997; *Hejl et al*., 1998, 2010; *Magganas et al*., 2004; *Wuthrich*, 2009; *Kounov et al*., 2010; *Márton et al*., 2010, and the results of this study] are summarized in the histograms of Figure 7. For the NRC low-temperature data are from both the migmatitic gneiss domes and their peripheries. With reference to the histograms of Figure 7, the zircon FT ages range from 25 to 40 Ma, the apatite FT ages from 10 to 50 Ma and the apatite (U-Th)/He ages from 10 to 40 Ma. For the SRCC the available data are less abundant. The zircon FT ages are from 10 to 45 Ma, the apatite FT ages from 5 to 30 Ma (both Oligo-Miocene plutons and basement rocks) and the three apatite (U-Th)/He ages from 15 to 40 Ma. For the Vertiskos Unit (or the equivalent Ograzden Unit) the two available zircon FT ages are at circa 80 Ma. The apatite FT ages of the Eocene plutons range from 10 to 40 Ma and from basements rocks from 40 to 70 Ma.

Much of the Mesozoic convergence that affected the Rhodope Metamorphic Province is preserved within the NRC. High-temperature zircon crystallization ages peak at Jurassic and is often interpreted as the time of the eclogite-facies metamorphism (in places within the diamond stability field). The eclogite-bearing gneisses of the NRC are variably retrogressed to amphibolite-facies conditions [see *Moulas et al*., 2013, and references therein]. The time of this event is constrained at Cretaceous [e.g., *Reischmann and Kostopoulos*, 2002; *Bauer et al*., 2007; *Bosse et al*., 2010; *Liati et al*., 2011; see also *Burg*, 2012, and references therein]. A second zircon/monazite growth phase scatters between uppermost Cretaceous and Oligocene and correlates with an elevated thermal gradient caused by voluminous intrusive and extrusive rocks (Figure 1). Simultaneously, widespread extensional basins deposited on top of exhumed metamorphic rocks, mark the initiation of extension in the Bulgarian Rhodope. The area remained active and at an elevated thermal gradient during the exhumation of the gneiss domes prevailing any pre-Lower Eocene (pre-50 Ma) low-temperature record. Indeed the low-temperature record starts at circa 50 Ma for the domes and their peripheries (Figure 7).

©2014. American Geophysical Union. All Rights Reserved.

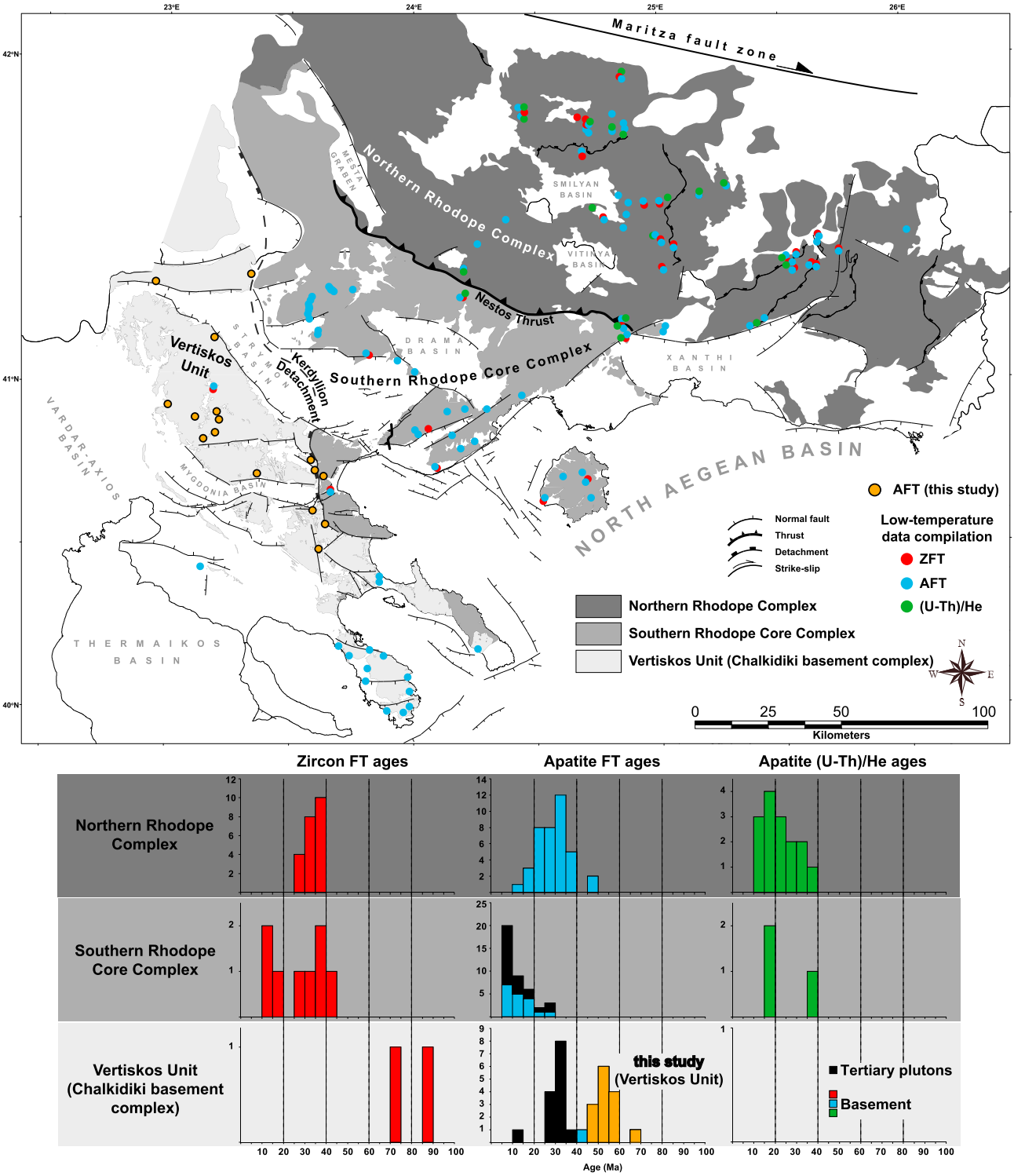

Figure 7. The Rhodope Metamorphic Province (Figure 1) is divided, from northeast to southwest, into three tectonic domains: The Northern Rhodope Complex (NRC), the Southern Rhodope Core Complex (SRCC), and the Vertiskos Unit. Low-temperature data compilation (ZFT, AFT, and (U-Th)/He) is shown on the map (orange-filled circles for our data; red-, blue-, and green-filled circles for literature data) and summarized in the histograms. The three tectonic domains are in gray-shaded colors as the corresponding histograms.

©2014. American Geophysical Union. All Rights Reserved.

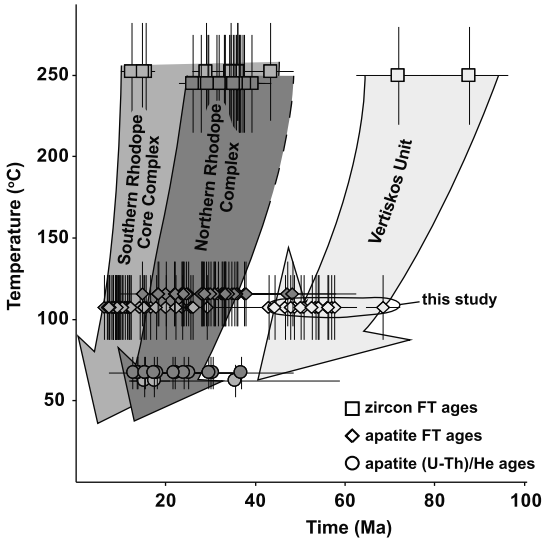

Figure 8. Simplified thermal paths (and data compilation) for the three tectonic domains shown in Figure 7. The available ZFT, AFT, and apatite (U-Th)/He ages are plotted against an "average" closure temperature (approximately 250, 110, and 60°C, respectively). The color fill of the three thermal paths (and the low-temperature data compilation) corresponds to the color fill of each of the three tectonic domains shown in Figure 7.

Similar to the NRC, the Vertiskos Unit preserves evidence for Upper Jurassic and Cretaceous metamorphism based on the available medium-temperature geochronology data mentioned earlier. Zircon FT ages (uppermost Cretaceous) predate the Eocene apatite FT ages for basement rocks (Figure 7). Contrary to the elevated thermal gradient in the NRC to the northeastern edge of the RMP, the Vertiskos Unit has been intruded only locally by plutonic bodies. Thus, the thermal history inferred from the FT data can be interpreted as a clear cooling signal of the basement block excluding any thermal overprint due to the plutons/volcanics emplacement. As described above, the Eocene and Oligo-Miocene plutonism and volcanism were not sufficient to increase the thermal gradient to such a degree to erase the evidence for the Upper Cretaceous exhumation. In addition, no significant-sized sedimentary basins have formed in the Vertiskos Unit which remained as a coherent basement zone to the southwest termination of the RMP.

This is in contrast to the SRCC where widespread extensional post middle Miocene basins developed on top of the exhumed metamorphic complex. As shown in Figure 7, the SRCC records the youngest population of ages (well illustrated in the apatite FT data with 20 samples with age $<$10 Ma) among the three domains of the RMP. The Eocene metamorphic ages, the Oligo-Miocene syntectonic intrusions and the relatively young low-temperature data point collectively toward a highly active area that remained at a high thermal gradient during the Tertiary before its fragmentation by post middle Miocene sedimentary basins. The relatively young ages of the SRCC attest for its denudation after both the NRC, to the northeast, and the Vertiskos Unit immediately to the southwest. The thermal gradient for the SRCC remained relatively high and only decreased sufficiently enough for low-temperature record to be preserved after upper Miocene times.

In summary, simple but distinct thermal paths (Figure 8) corresponding to the three tectonic domains of the RMP (Figure 7) can be defined. To the southwest, the Vertiskos Unit records Upper Cretaceous exhumation (Figures 4 and 6). No later episodes of pluton intrusion and basin formation erased the evidence for this exhumation. To the northeast, the NRC is characterized by high thermal gradient due to Upper Cretaceous-Oligocene intrusive and extrusive rocks, gneissic domes formation often accompanied with Eocene partial melting and basin development since Maastrichtian. The elevated thermal regime prevented any pre-Eocene exhumation phase to be recorded by low-temperature thermochronological systems. However, a lowermost Paleocene cooling phase is locally inferred from medium-temperature geochronology (Ar/Ar on white micas) on the hanging walls of the exhuming domes and is in line with Maastrichtian-Eocene syntectonic clastics deposited on the metamorphic basement [*Bonev et al.*, 2006, 2013a]. Finally, the intermediate SRCC provides the record of the youngest cooling history in the area in agreement with young syntectonic plutonism.

7. Conclusions

The Vertiskos Unit of the Chalkidiki peninsula (Figure 1) is a distinct Silurian fragment of Gondwanan provenance with a complex poly-metamorphic history. Its Alpine thermal history is documented by the available medium-temperature geochronology data that culminates in the Lower Cretaceous and is often correlated to a lower amphibolite-facies overprint. In an effort to constrain its post-Lower

©2014. American Geophysical Union. All Rights Reserved.

Cretaceous cooling history until close-to-surface temperature, we applied apatite FT analysis coupled with inverse thermal modeling. Our results can be summarized as

1. The central ages obtained for basement rocks of the Vertiskos Unit range from uppermost Cretaceous to middle Eocene (46.6 ± 3.6 to 68.5 ± 3.8 Ma) with mean track lengths between 13 and 13.5 μm (Table 1).
2. In the Vertiskos Unit there is potentially a geographic trend for younger AFT ages toward the east (Figure 5). This trend becomes less well defined when considered in the context of the age uncertainties (overlapping ages within error). This suggests that either the AFT dating is not sensitive enough to record clearly such variation over such a narrow width (~35 Km) or that the observed pattern simply reflects scatter in the data. In the lack of any conclusive evidence, we have chosen to (a) model each sample independently examining this geographical trend and (b) model the thermal history of all samples together treating them as a vertical profile and interpreting the geographical trend as an artifact. To assess whether the geographical variation in the AFT ages is real, a more dense sampling grid coupled with both lower ([U-Th]/He) and higher-temperature methods (Ar/Ar on potassic feldspars, ZFT) would be necessary.
3. However, both of the modeling approaches produced similar results in terms of form of the cooling path and timing (crossing the high-temperature limit of the PAZ; near-surface exposure). Considering the Vertiskos Unit and independently of the chosen modeling approach, its overall thermal history implies that it cooled through the apatite PAZ in uppermost Cretaceous and was at near-surface temperature (less than 50°C) by lower/middle Eocene (Figures 4 and 6). Thus, the Vertiskos Unit preserves the evidence for uppermost Cretaceous exhumation.
4. The Vertiskos Unit is the westernmost extreme of the Rhodope Metamorphic Province (Figure 7). The other constituents are the Southern Rhodope Core Complex in the center and the Northern Rhodope Complex to the northeast. The inferred thermal evolution of the Vertiskos Unit (Figures 4 and 6) is in contrast to the one of the Southern Rhodope Core Complex and the Northern Rhodope Complex where the apatite fission track ages range from circa 10 to 30 Ma and from circa 10 to 40 Ma, respectively (Figure 7). Figure 8 summarizes, in a simplified way, the distinct thermal paths of the three tectonic domains of the Rhodope Metamorphic Province (Figure 7). It shows clearly the difference in terms of timing of close-to-surface exposure between them and establishes Vertiskos Unit as the oldest exhumed basement complex in the Rhodope. We can also safely conclude that the Vertiskos Unit represents the oldest exhumed coherent basement complex of Greece.

Acknowledgments
This work was funded by the European Union FP7 Marie Curie ITN "TOPOMOD" contract 264517. Andrew Carter and Jocelyn Barbarand are gratefully acknowledged for providing access to the FT microscopes at Birkbeck University of London and Géosciences Orsay, Université Paris Sud, respectively. We thank Ewald Hejl for kindly providing us with the necessary data for the inverse modeling of the Eocene Sithonia granite shown in Figure 5. Editorial handling by Claudio Faccenna is greatly appreciated. Nikolay Bonev and Ewald Hejl are thanked for their valuable suggestions and critical comments that greatly improved our manuscript.

References

Balestrieri, M. L., E. Pandeli, G. Bigazzi, R. Carosi, and C. Montomoli (2011), Age and temperature constraints on metamorphism and exhumation of the syn-orogenic metamorphic complexes of Northern Apennines, Italy, *Tectonophysics*, *509*(3–4), 254–271, doi:10.1016/j.sedgeo.2013.02.010.

Balestrieri, M., M. Benvenuti, and F. Tangocci (2013), Detrital fission-track-compositional signature of an orogenic chain-hinterland basin system: The case of the late Neogene Quaternary Valdelsa basin (Northern Apennines, Italy), *Sediment. Geol.*, *289*, 159–168, doi:10.1016/j.tecto.2011.06.015.

Barbarand, J., F. Lucazeau, M. Pagel, and M. Seranne (2001), Burial and exhumation history of the south-eastern Massif Central (France) constrained by apatite fission-track thermochronology, *Tectonophysics*, *335*(3–4), 275–290, doi:10.1016/S0040-1951(01)00069-5.

Barbarand, J., A. Carter, I. Wood, and T. Hurford (2003), Compositional and structural control of fission-track annealing in apatite, *Chem. Geol.*, *198*(1–2), 107–137, doi:10.1016/S0009-2541(02)00424-2.

Bauer, C., D. Rubatto, K. Krenn, A. Proyer, and G. Hoinkes (2007), A zircon study from the Rhodope metamorphic complex, N-Greece: Time record of a multistage evolution, *Lithos*, *99*(3–4), 207–228.

Bernet, M., and J. I. Garver (2005), Fission-track analysis of detrital zircon, *Rev. Mineral. Geochem.*, *58*(1), 205–237, doi:10.2138/rmg.2005.58.8.

Bigazzi, S. G., G. Christofides, A. D. Moro, and C. Kyriakopoulos (1994), A contribution to the evolution of the Xanthi pluton (northern Greece): The apatite fission track analysis, *Boll. Soc. Geol. It.*, *113*, 243–248.

Bonev, N., and Y. Dilek (2010), Geochemistry and tectonic significance of proto-ophiolitic metamafic units from the Serbo-Macedonian and western Rhodope massifs (Bulgaria- Greece), *Int. Geol. Rev.*, *52*(2–3), 298–335, doi:10.1080/00206810902757214.

Bonev, N., J.-P. Burg, and Z. Ivanov (2006), Mesozoic-Tertiary structural evolution of an extensional gneiss dome—The Kesebir-Kardamos dome, eastern Rhodope (Bulgaria-Greece), *Int. J. Earth Sci. (Geol Rundsch)*, *95*(2), 318–340, doi:10.1007/s00531-005-0025-y.

Bonev, N., R. Spikings, R. Moritz, and P. Marchev (2010), The effect of early Alpine thrusting in late-stage extensional tectonics: Evidence from the Kulidzhik nappe and the Pelevun extensional allochthon in the Rhodope Massif, Bulgaria, *Tectonophysics*, *488*(1–4), 256–281.

Bonev, N., R. Spikings, R. Moritz, P. Marchev, and D. Collings (2013a), $^{40}Ar/^{39}Ar$ age constraints on the timing of Tertiary crustal extension and its temporal relation to ore-forming and magmatic processes in the Eastern Rhodope Massif, Bulgaria, *Lithos*, *180–181*, 264–278.

Bonev, N., M. Ovtcharova-Schaltegger, R. Moritz, P. Marchev, and A. Ulianov (2013b), Peri-Gondwanan Ordovician crustal fragments in the high-grade basement of the Eastern Rhodope Massif, Bulgaria: Evidence from U-Pb LA-ICP-MS zircon geochronology and geochemistry, *Geodinamica Acta*, doi:10.1080/09853111.2013.858942.

Bosse, V., Z. Cherneva, P. Gautier, and I. Gerdjikov (2010), Two partial melting events as recorded by the U-Th-Pb chronometer in monazite: LA-ICPMS in situ dating in metapelites from the Bulgarian Central Rhodopes, *Geol. Balc.*, *39*(1–2), 51–52.

Boyanov, I., M. Ruseva, and E. Dimitrova (1982), First find of Upper-Cretaceous foraminifers in East-Rhodopes, *Geol. Balc.*, *12*(4), 20.

Brun, J.-P., and D. Sokoutis (2007), Kinematics of the Southern Rhodope Core Complex (North Greece), *Int. J. Earth Sci. (Geol Rundsch)*, *96*(6), 1079–1099, doi:10.1007/s00531-007-0174-2.

©2014. American Geophysical Union. All Rights Reserved.

Burchfiel, B. C., R. Nakov, N. Dumurdzanov, D. Papanikolaou, T. Tzankov, T. Serafimovski, R. W. King, V. Kotzev, A. Todosov, and B. Nurce (2008), Evolution and dynamics of the Cenozoic tectonics of the South Balkan extensional system, *Geosphere*, *4*(6), 919–938, doi:10.1130/GES00169.1.

Burchfiel, C. B., R. Nakov, T. Tzankov, and L. H. Royden (2000), Cenozoic extension in Bulgaria and northern Greece: The northern part of the Aegean extensional regime, *Geol. Soc. London Spec. Publ.*, *173*, 325–352.

Burg, J.-P. (2012), Rhodope: From Mesozoic convergence to Cenozoic extension. Review of petro-structural data in the geochronological frame, *J. Virtual Explorer*, *42*(1), doi:10.3809/jvirtex.2011.00270.

Burg, J.-P., Z. Ivanov, L.-E. Ricou, D. Dimov, and L. Klain (1990), Implications of shear-sense criteria for the tectonics evolution of the Central Rhodope massif, southern Bulgaria, *Geology*, *18*, 451–454, doi:10.1130/0091-7613(1990)018.

Burg, J.-P., I. Godfriaux, and L.-E. Ricou (1995), Extension of the Mesozoic Rhodope thrust units in the Vertiskos-Kerdilion Massifs, *C. R. Acad. Sci. Paris*, *320*(IIa), 889–896.

Burg, J.-P., L.-E. Ricou, Z. Ivanov, I. Godfriaux, D. Dimov, and L. Klain (1996), Syn-metamorphic nappe complex in the Rhodope Massif. Structure and kinematics, *Terra Nova*, *8*(1), 6–15, doi:10.1111/j.1365-3121.1996.tb00720.x.

Carlson, W. D., R. A. Donelick, and R. A. Ketcham (1999), Variability of apatite fission-track annealing kinetics; I. Experimental results, *Am. Mineral.*, *84*(9), 1213–1223.

Carrapa, B. (2009), Tracing exhumation and orogenic wedge dynamics in the European Alps with detrital thermochronology, *Geology*, *37*(12), 1127–1130, doi:10.1130/G30065A.1.

Carter, A. (1999), Present status and future avenues of source region discrimination and characterization using fission track analysis, *Sediment. Geol.*, *124*, 31–45.

Charvin, K., K. Gallagher, G. L. Hampson, and R. Labourdette (2009), A Bayesian approach to inverse modelling of stratigraphy. Part 1: Method, *Basin Res.*, *51*, 5–25, doi:10.1111/j.1365-2117.2008.00369.x.

Christofides, G., C. D'Amico, A. D. Moro, G. Eleftheriadis, and C. Kyriakopoulos (1990), Rb/Sr geochronology and geochemical characters of the Sithonia plutonic complex (Greece), *Eur. J. Mineral.*, *2*, 79–87.

Cogne, N., K. Gallagher, and P. R. Cobbold (2011), Post-rift reactivation of the onshore margin of southeast Brazil: Evidence from apatite (U-Th)/He and fission-track data, *Earth Planet. Sci. Lett.*, *309*, 118–130, doi:10.1016/j.epsl.2011.06.025.

Cogne, N., K. Gallagher, P. R. Cobbold, C. Riccomini, and C. Gautheron (2012), Post- breakup tectonics in southeast Brazil from thermochronological data and combined inverse-forward thermal history modeling, *J. Geophys. Res.*, *117*, B11413, doi:10.1029/2012JB009340.

de Wet, A. P., J. A. Miller, M. J. Bickle, and H. J. Chapman (1989), Geology and geochronology of the Arnea, Sithonia and Ouranopolis intrusions, Chalkidiki Peninsula, northern Greece, *Tectonophysics*, *161*(1–2), 65–79, doi:10.1016/0040-1951(89)90303-X.

Dimitrijevic, M. (1963), Sur l'âge du métamorphism et des plissements dans la masse Serbo- Macédoniènne, in *Proc. VI Congr. Carp. Balk. Geol. Assoc.*, pp. 339–347.

Dinter, D. A., and L. Royden (1993), Late Cenozoic extension in northeastern Greece: Strymon Valley detachment system and Rhodope metamorphic core complex, *Geology*, *21*, 45–48, doi:10.1130/0091-7613(1993)021.

Dinter, D. A., A. Macfarlane, W. Hames, C. Isachsen, S. Bowring, and L. Royden (1995), U-Pb and $^{40}Ar/^{39}Ar$ geochronology of the Symvolon granodiorite: Implications for the thermal and structural evolution of the Rhodope metamorphic core complex, northeastern Greece, *Tectonics*, *14*(4), 886–908, doi:10.1029/95TC00926.

Donelick, R., P. O'Sullivan, and R. Ketcham (2005), Apatite fission-track analysis, *Rev. Mineral. Geochem.*, *58*, 49–94, doi:10.2138/rmg.2005.58.3.

Dörr, N., F. Lisker, P. D. Clift, A. Carter, D. G. Gee, A. M. Tebenkov, and C. Spiegel (2012), Late Mesozoic-Cenozoic exhumation history of northern Svalbard and its regional significance: Constraints from apatite fission track analysis, *Tectonophysics*, *514–517*, 81–92, doi:10.1016/j.tecto.2011.10.007.

Dunkl, I. (2002), Trackkey: A Windows program for calculation and graphical presentation of fission track data, *Comput. Geosci.*, *28*(1), 3–12, doi:10.1016/S0098-3004(01)00024-3.

Eleftheriadis, G., W. Frank, and K. Petrakakis (2001), $^{40}Ar/^{39}Ar$ dating and cooling history of the Pangeon granitoids, Rhodope Massif (eastern Macedonia, Greece), *Bull. Geol. Soc. Greece*, *XXXIV*(3), 911–916.

Filipov, P., and P. Marchev (2011), U-Pb zircon and $^{40}Ar/^{39}Ar$ ages of Mesta volcanic rocks and Central Pirin pluton, in Bulgarian National Conference "GEOSCIENCES 2011".

Foster, D. A., and A. Raza (2002), Low-temperature thermochronological record of exhumation of the Bitterroot metamorphic core complex, northern Cordilleran Orogen, *Tectonophysics*, *349*(1–4), 23–36, doi:10.1016/S0040-1951(02)00044-6.

Frei, D. (1996), The extent of inter-mineral isotope equilibrium: a systematic bulk U-Pb and Pb step leaching (PbSL) isotope study of individual minerals from the Tertiary granite of Jerissos (northern Greece), *Eur. J. Mineral.*, *8*, 1175–1189.

Frei, R. (1992), Isotope (Pb,Rb-Sr,S,O,C,U-Pb) geochemical investigations on Tertiary intrusives and related mineralizations in the Serbomacedonian Pb-Zn, Sb+Cu-Mo metallogenetic province in Northern Greece, PhD thesis, Swiss Federal Institute of Technology (ETH), Zurich.

Galbraith, R., and G. Laslett (1993), Statistical models for mixed fission track ages, *Nucl. Tracks Radiat. Meas.*, *21*(4), 459–470, doi:10.1016/1359-0189(93)90185-C.

Gallagher, K. (2012), Transdimensional inverse thermal history modeling for quantitative thermochronology, *J. Geophys. Res.*, *117*, B02408, doi:10.1029/2011JB008825.

Gallagher, K., R. Brown, and C. Johnson (1998), Fission track analysis and its applications to geological problems, *Annu. Rev. Earth Planet. Sci.*, *26*, 519–572.

Gallagher, K., J. Stephenson, R. Brown, C. Holmes, and P. Ballester (2005a), Exploiting 3d spatial sampling in inverse modeling of thermochronological data, *Rev. Mineral. Geochem.*, *58*(1), 375–387, doi:10.2138/rmg.2005.58.14.

Gallagher, K., J. Stephenson, R. Brown, C. Holmes, and P. Fitzgerald (2005b), Low temperature thermochronology and modeling strategies for multiple samples 1: Vertical profiles, *Earth Planet. Sci. Lett.*, *237*(1–2), 193–208, doi:10.1016/j.epsl.2005.06.025.

Gallagher, K., K. Charvin, S. Nielsen, M. Sambridge, and J. Stephenson (2009), Markov chain Monte Carlo (MCMC) sampling methods to determine optimal models, model resolution and model choice for Earth Science problems, *Mar. Pet. Geol.*, *26*, 525–535, doi:10.1016/j.marpetgeo.2009.01.003.

Gilg, H. A., and R. Frei (1994), Chronology of magmatism and mineralization in the Kassandra mining area, Greece: The potentials and limitations of dating hydrothermal illites, *Geochim. Cosmochim. Acta*, *58*(9), 2107–2122.

Gleadow, A. J. W. (1981), Fission track dating methods: What are the real alternatives?, *Nucl. Tracks*, *5*(1–2), 3–14, doi:10.1016/0191-278x(81)90021-4.

Goranov, A., and G. Atanasov (1992), Lithostratigraphy and formation conditions of Maastrichtian-Paleocene deposits in Krumovgrad District, *Geol. Balc.*, *22*(3), 71–82.

Gunnell, Y., K. Gallagher, A. Carter, M. Widdowson, and A. J. Hurford (2003), Denudation history of the continental margin of western peninsular India since the early Mesozoic—Reconciling apatite fission-track data with geomorphology, *Earth Planet. Sci. Lett.*, *215*(1–2), 187–201, doi:10.1016/S0012-821X(03)00380-7.

©2014. American Geophysical Union. All Rights Reserved.

Harkovska, A., P. S. Petrov, Z. Milakovska, and V. Nakova (2010), "Kozhuh volcano" (SW Bulgaria)—Arrangement of the puzzle, 2010 [in Bulgarian], *Rev. Bulg. Geol. Soc.*, *71*(1–3), 149–166.

Harre, W., F. Kockel, H. Kreuzer, H. Lenz, P. Müller, and H. W. Walther (1968), Uber Rejuvenationen im Serbo-Madzedonischen Massiv (Deutung radiometrischer Altersbes-timmungen), in *XXIII International Geological Congress*, vol. 6, pp. 223–236, Prague, Czechoslovakia.

Hejl, E., H. Weingartner, E. Vavliakis, and A. Psilovikos (1998), Macrorelief features and fission-track thermochronology of the Rila-Rhodope massif (Eastern Macedonia, Greece), *Zeitschrift für Geomorphologie, NF*, *42*(4), 517–530.

Hejl, E., M. Bernroider, O. Parlak, and H. Weingartner (2010), Fission-track thermochronology, vertical kinematics, and tectonic development along the western extension of the North Anatolian Fault zone, *J. Geophys. Res.*, *115*, B10407, doi:10.1029/2010JB007402.

Himmerkus, F., P. Zachariadis, T. Reischmann, and D. Kostopoulos (2005), The mafic complexes of the Athos-Volvi-Zone—A suture zone between the Serbo-Macedonian Massif and the Rhodope Massif?, *Geophys. Res. Abstr.*, *7*, 10,240.

Himmerkus, F., T. Reischmann, and D. Kostopoulos (2006), Late Proterozoic and Silurian basement units within the Serbo-Macedonian Massif, northern Greece: The significance of terrane accretion in the Hellenides, *Geol. Soc. London Spec. Publ.*, *260*, 35–50.

Himmerkus, F., T. Reischmann, and D. Kostopoulos (2009a), Serbo-Macedonian revisited: A Silurian basement terrane from northern Gondwana in the Internal Hellenides, Greece, *Tectonophysics*, *473*(1–2), 20–35, doi:10.1016/j.tecto.2008.10.016.

Himmerkus, F., T. Reischmann, and D. Kostopoulos (2009b), Triassic rift-related meta-granites in the Internal Hellenides, Greece, *Geol. Mag.*, *146*(2), 252–265, doi:10.1017/S001675680800592X.

Himmerkus, F., P. Zachariadis, T. Reischmann, and D. Kostopoulos (2012), The basement of the Mount Athos peninsula, northern Greece: Insights from geochemistry and zircon ages, *Int. J. Earth Sci. (Geol Rundsch)*, *101*(6), 1467–1485, doi:10.1007/s00531-011-0644-4.

Hoinkes, G., E. Krenn, D. Rubatto, K. Krenn, A. Proyer, F. Bernhard, and C. Bauer (2008), Timing the Rhodope UHP-event using zircon and monazite, in 33rd International Geological Congress. UHP-04 Ultra-high pressure metamorphism: Mineral reactions, geochemistry, thermobarometry and geochronology.

Hopcroft, P. O., K. Gallagher, and C. C. Pain (2007), Inference of past climate from borehole temperature data using Bayesian Reversible Jump Markov chain Monte Carlo, *Geophys. J. Int.*, *171*(3), 1430–1439, doi:10.1111/j.1365-246X.2007.03596.x.

Hurford, A. J., and P. F. Green (1982), A users' guide to fission track dating calibration, *Earth Planet. Sci. Lett.*, *59*(2), 343–354, doi:10.1016/0012-821x(82)90136-4.

Hurford, A. J., and P. F. Green (1983), The zeta age calibration of fission-track dating, *Chem. Geol.*, *41*, 285–317, doi:10.1016/S0009-2541(83)80026-6.

Jahn-Awe, S., N. Froitzheim, T. J. Nagel, D. Frei, N. Georgiev, and J. Pleuger (2010), Structural and geochronological evidence for Paleogene thrusting in the western Rhodopes, SW Bulgaria: Elements for a new tectonic model of the Rhodope Metamorphic Province, *Tectonics*, *29*, TC3008, doi:10.1029/2009TC002558.

Jahn-Awe, S., J. Pleuger, D. Frei, N. Georgiev, N. Froitzheim, and T. J. Nagel (2012), Time constraints for low-angle shear zones in the Central Rhodopes (Bulgaria) and their significance for the exhumation of high-pressure rocks, *Int. J. Earth Sci. (Geol Rundsch)*, *101*(7), 1971–2004, doi:10.1007/s00531-012-0764-5.

Janák, M., N. Froitzheim, N. Georgiev, T. J. Nagel, and S. Sarov (2011), P-T evolution of kyanite eclogite from the Pirin Mountains (SW Bulgaria): Implications for the Rhodope UHP Metamorphic Complex, *J. Metamorph. Geol.*, *29*(3), 317–332, doi:10.1111/j.1525-1314.2010.00920.x.

Jolivet, L., and J.-P. Brun (2010), Cenozoic geodynamic evolution of the Aegean, *Int. J. Earth Sci. (Geol Rundsch)*, *99*(1), 109–138, doi:10.1007/s00531-008-0366-4.

Jolivet, M., P. Labaume, P. Monie, M. Brunel, N. Arnaud, and M. Campani (2007), Thermochronology constraints for the propagation sequence of the south Pyrenean basement thrust system (France-Spain), *Tectonics*, *26*, TC5007, doi:10.1029/2006TC002080.

Jolivet, M., S. Dominguez, J. Charreau, Y. Chen, Y. Li, and Q. Wang (2010), Mesozoic and Cenozoic tectonic history of the central Chinese Tian Shan: Reactivated tectonic structures and active deformation, *Tectonics*, *29*, TC6019, doi:10.1029/2010TC002712.

Jones, C. E., J. Tarney, J. H. Baker, and F. Gerouki (1992), Tertiary granitoids of Rhodope, northern Greece: Magmatism related to extensional collapse of the Hellenic Orogen?, *Tectonophysics*, *210*(3–4), 295–314, doi:10.1016/0040-1951(92)90327-3.

Kaiser-Rohrmeier, M., A. von Quadt, T. Driesner, C. A. Heinrich, R. Handler, M. Ovtcharova, Z. Ivanov, P. Petrov, S. Sarov, and I. Peytcheva (2013), Post-orogenic extension and hydrothermal ore formation: High-precision geochronology of the central rhodopian metamorphic core complex (Bulgaria-Greece), *Econ. Geol.*, *108*(4), 691–718.

Kauffmann, G., F. Kockel, and H. Mollat (1976), Notes on the stratigraphic and paleogeographic position of the Svoula Formation in the Innermost Zone of the Hellenides (Northern Greece), *Bull. Soc. Geol. France*, *7*(2), 225–230.

Kaufman, P. S. (1995), Extensional tectonic history of the Rhodope Metamorphic Core Complex, Greece and geophysical modeling of the Halloran Hills, California, PhD thesis, Massachusetts Institute of Technology.

Ketcham, R. A., A. Carter, R. A. Donelick, J. Barbarand, and A. J. Hurford (2007), Improved modeling of fission-track annealing in apatite, *Am. Mineral.*, *92*, 799–810.

Kilias, A., G. Falalakis, and D. Mountrakis (1999), Cretaceous-Tertiary structures and kinematics of the Serbomacedonian metamorphic rocks and their relation to the exhumation of the Hellenic hinterland (Macedonia, Greece), *Int. J. Earth Sci. (Geol Rundsch)*, *88*(3), 513–531, doi:10.1007/s005310050282.

Kockel, F., H. Mollat, and H. W. Walther (1971), Geologie des Serbe-Mazedonischen Massivs und seines mesozoischen Rahmens (Nordgriechenland), *Geol. Jb.*, *89*(1), 529–551.

Kockel, F., and H. Mollat (1977), Geological map of the Chalkidiki peninsula and adjacent areas (Greece), Scale 1: 100000, Bundesanstalt fur Geowissenschaften und Rohstoffe, Hannover.

Kockel, F., H. Mollat, and H. Walther (1977), *Erlauterungen zur Geologischen Karte der Chalkidiki und Angrenzender Gebiete*, vol. 119, Bundesanstalt für Geowissenschaften und Rohstoffe, Hannover.

Kolocotroni, C., and J. E. Dixon (1991), The origin and emplacement of the Vrondou granite, Serres, NE Greece, *Bull. Geol. Soc. Greece*, *XXV*(1), 469–483.

Koufos, G. D., G. E. Syrides, D. S. Kostopoulos, and K. K. Koliadimou (1995), Preliminary results about the stratigraphy and the palaeoenvironment of Mygdonia Basin, Macedonia, Greece, *Geobios*, *18*, 243–249.

Kounov, A., D. Seward, J.-P. Burg, D. Bernoulli, Z. Ivanov, and R. Handler (2010), Geochronological and structural constraints on the Cretaceous thermotectonic evolution of the Kraishte zone, western Bulgaria, *Tectonics*, *29*, TC2002, doi:10.1029/2009TC002509.

Kounov, A., J. Graf, A. von Quadt, D. Bernoulli, J.-P. Burg, D. Seward, Z. Ivanov, and C. M. Fanning (2012), Evidence for a "Cadomian" ophiolite and magmatic-arc complex in SW Bulgaria, *Precambrian Res.*, *212–213*, 275–295.

Krenn, K., C. Bauer, A. Proyer, U. Klötzli, and G. Hoinkes (2010), Tectonometamorphic evolution of the Rhodope orogen, *Tectonics*, *29*, TC4001, doi:10.1029/2009TC002513.

Kydonakis, K., D. Kostopoulos, M. Poujol, J.-P. Brun, D. Papanikolaou, and J.-L. Paquette (2014), The dispersal of the Gondwana Super-fan System in the eastern Mediterranean: New insights from detrital zircon geochronology, *Gondwana Res.*, *25*(25), 1230–1241, doi:10.1016/j.gr.2013.05.009.

©2014. American Geophysical Union. All Rights Reserved.

Kyriakopoulos, K. G., A. C. Magganas, P. Norelli, G. Bigazzi, A. D. Moro, and A. Kokkinakis (1997), Thermochronological evolution of Symvolon and Pangeon pluton and their country rocks, Kavala area, N. Greece: An apatite fission track analysis, *N. Jb. Miner. Mh.*, *H11*, 519–529.

Labaume, P., M. Jolivet, F. Souquiere, and A. Chauvet (2008), Tectonic control on diagenesis in a foreland basin: Combined petrologic and thermochronologic approaches in the Gres d'Annot basin (Late Eocene-Early Oligocene, French-Italian external Alps), *Terra Nova*, *20*(2), 95–101, doi:10.1111/j.1365-3121.2008.00793.x.

Leech, M. L., and D. Stockli (2000), The late exhumation history of the ultrahigh-pressure Maksyutov Complex, south Ural Mountains, from new apatite fission track data, *Tectonics*, *19*(1), 153–167, doi:10.1029/1999TC900053.

Liati, A., and E. Seidel (1996), Metamorphic evolution and geochemistry of kyanite eclogites in central Rhodope, northern Greece, *Contrib. Mineral. Petrol.*, *123*(3), 293–307, doi:10.1007/s004100050157.

Liati, A., D. Gebauer, and C. M. Fanning (2011), Ultrahigh-pressure metamorphism: 25 years after the discovery of coesite and diamond, chap. in *Geochronology of the Alpine UHP Rhodope Zone: A Review of Isotopic Ages and Constraints on the Geodynamic Evolution*, pp. 295–324, Elsevier Inc., Amsterdam, doi:10.1016/B978-0-12-385144-4.00009-6.

Lilov, P., I. Zagorcev, and I. Peeva (1983), Rubidium-strontium isochron data on the age of the metamorphism of the Ograždenian Complex, Maleševska Mountain, *Geol. Balc.*, *13*(2), 31–40.

Lips, A. L. W., S. H. White, and J. R. Wijbransb (2000), Middle-Late Alpine thermotectonic evolution of the southern Rhodope Massif, Greece, *Geodinamica Acta*, *13*, 281–292.

Macheva, L., I. Peycheva, A. von Quadt, N. Zidarov, and E. Tarassova (2006), Petrological, geochemical and isotope features of Lozen metagranite, Belasitza Mountain—Evidence for widespread distribution of Ordovician metagranitoids in the Serbo-Macedonian Massif, SW Bulgaria, in Bulgarian National Conference "GEOSCIENCES 2006".

Magganas, A., G. Bigazzi, K. Kyriakopoulos, and M. L. Balestrieri (2004), Low-T thermochronological evolution of the Vrondou composite pluton (northern Greece) using apatite fission track analysis, in 5th International Symposium on Eastern Mediterranean Geology Thessaloniki, Greece, 14–20 April.

Marakis, G. (1969), Geochronology of granites from Macedonia (Greece) [in Greek], *Ann. Geol. des Pays Helleniques*, *21*, 121–152.

Marchev, P., R. Raicheva, H. Downes, O. Vaselli, M. Chiaradia, and R. Moritz (2004), Compositional diversity of Eocene-Oligocene basaltic magmatism in the Eastern Rhodopes, SE Bulgaria: Implications for genesis and tectonic setting, *Tectonophysics*, *393*(1–4), 301–328, doi:10.1016/j.tecto.2004.07.045.

Marchev, P., A. von Quadt, I. Peytcheva, and M. Ovtcharova (2006), The age and origin of the Chuchuliga and Rozino granites, Eastern Rhodopes, in Bulgarian National Conference "GEOSCIENCES 2006".

Marchev, P., P. Kibarov, R. Spikings, M. Ovtcharova, I. Marton, and R. Moritz (2010), $^{40}Ar/^{39}Ar$ and U-Pb geochronology of the Iran Tepe volcanic complex, Eastern Rhodopes, *Geol. Balc.*, *39*(3), 3–12.

Marchev, P., S. Georgiev, R. Raicheva, I. Peytcheva, A. von Quadt, M. Ovtcharova, and N. Bonev (2013), Adakitic magmatism in post-collisional setting: An example from the early-middle Eocene magmatic belt in southern Bulgaria and northern Greece, *Lithos*, *180–181*, 159–180, doi:10.1016/j.lithos.2013.08.024.

Márton, I., R. Moritz, and R. Spikings (2010), Application of low-temperature thermochronology to hydrothermal ore deposits: Formation, preservation and exhumation of epithermal gold systems from the Eastern Rhodopes, Bulgaria, *Tectonophysics*, *483*(3–4), 240–254, doi:10.1016/j.tecto.2009.10.020.

Meinhold, G., D. Kostopoulos, T. Reischmann, D. Frei, and M. K. BouDagher-Fadel (2009), Geochemistry, provenance and stratigraphic age of metasedimentary rocks from the eastern Vardar suture zone, northern Greece, *Palaeogeogr. Palaeoclimatol. Palaeoecol.*, *277*, 199–225, doi:10.1016/j.palaeo.2009.04.005.

Moulas, E., D. Kostopoulos, J. A. D. Connolly, and J.-P. Burg (2013), P-T estimates and timing of the sapphirine-bearing metamorphic overprint in kyanite eclogites from Central Rhodope, northern Greece, *Petrology*, *21*(5), 507–521.

Mposkos, E., and A. Liati (1993), Metamorphic evolution of metapelites in the high-pressure terrane of the Rhodope Zone, Northern Greece, *Can. Mineral.*, *31*, 401–424.

Mposkos, E. D., and D. K. Kostopoulos (2001), Diamond, former coesite and supersilicic garnet in metasedimentary rocks from the Greek Rhodope: A new ultrahigh-pressure metamorphic province established, *Earth Planet. Sci. Lett.*, *192*(4), 497–506, doi:10.1016/S0012-821X(01)00478-2.

Nagel, T. J., S. Schmidt, M. Janak, N. Froitzheim, S. Jahn-Awe, and N. Georgiev (2011), The exposed base of a collapsing wedge: The Nestos Shear Zone (Rhodope Metamorphic Province, Greece), *Tectonics*, *30*, TC4009, doi:10.1029/2010TC002815.

Ovtcharova, M., A. von Quadt, C. A. Heinrich, M. Frank, M. Kaiser-Rohrmeier, I. Peycheva, and Z. Cherneva (2003), Triggering of hydrothermal ore mineralization in the Central Rhodopean Core Complex (Bulgaria)—Insight from isotope and geochronological studies on tertiary magmatism and migmatization, in *7th Biennial Meeting, Society for Geology Applied to Mineral Deposits, Mineral Exploration and Sustainable Development*, pp. 367–370, Mill press, Rotterdam.

Papadopoulos, C., and A. Kilias (1985), Altersbeziehungen zwischen metamorphose und deformation im zentralen Teil des Serbomazedonischen Massivs (Vertiskos Gebirge, Nord- Griechenland) [in German with English abstract], *Geol. Rundsch.*, *74*(1), 77–85.

Papanikolaou, D. J. (2013), Tectonostratigraphic models of the Alpine terranes and subduction history of the Hellenides, *Tectonophysics*, *595–596*, 1–24, doi:10.1016/j.tecto.2012.08.008.

Papanikolaou, D., M. Alexandri, and P. Nomikou (2006), Active faulting in the north Aegean basin, *Geol. Soc. Spec. Pap.*, *409*, 189–209, doi:10.1130/2006.2409(11).

Pecskay, Z., A. Harkovska, P. S. Petrov, and M. Popov (2011), K-Ar dating of Kozhuh volcanic body (SW Bulgaria), *C. R. Acad. Bulg. Sci.*, *64*(2), 263–268.

Perraki, M., A. Proyer, E. Mposkos, R. Kaindl, and G. Hoinkes (2006), Raman micro-spectroscopy on diamond, graphite and other carbon polymorphs from the ultrahigh- pressure metamorphic Kimi Complex of the Rhodope Metamorphic Province, NE Greece, *Earth Planet. Sci. Lett.*, *241*(3–4), 672–685, doi:10.1016/j.epsl.2005.11.014.

Peytcheva, I., Y. Kostitsin, E. Salnikova, B. Kamenov, and L. Klain (1998), Rb-Sr and U-Pb isotope data for the Rila-Rhodope batholith [in Bulgarian with English abstract], *Geochem., Mineral. Petrol.*, *35*, 93–105.

Poli, G., G. Christo des, A. Koroneos, T. Soldatos, D. Perugini, and A. Langone (2009), Early Triassic granitic magmatism—Arnea and Kerkini granitic complexes—In Vertiskos Unit (Serbo-Macedonian Massif, north-eastern Greece) and its significance in the geodynamic evolution of the area, *Acta Volcanologica*, *20–21*(1–2), 47–70.

Reischmann, T., and D. Kostopoulos (2002), Timing of UHPM in metasediments from the Rhodope Massif, N Greece, in Goldschmidt Conference Abstracts, no. A634.

Ricou, L.-E., and I. Godfriaux (1994), The Thessaloniki klippe: A nappe of Vertiskos orogin emplaced upon the Mesozoic ysches of the Vardar basin, *Bull. Geol. Soc. Greece*, *XXX*(1), 69–78.

©2014. American Geophysical Union. All Rights Reserved.

Ricou, L.-E., J.-P. Burg, I. Godfriaux, and Z. Ivanov (1998), Rhodope and Vardar: The metamorphic and the olistostromic paired belts related to the Cretaceous subduction under Europe, *Geodinamica Acta*, *11*(6), 285–309.

Ring, U., J. Glodny, T. Will, and S. Thomson (2010), The Hellenic subduction system: High-pressure metamorphism, exhumation, normal faulting, and large-scale extension, *Annu. Rev. Earth Planet. Sci.*, *38*, 45–76, doi:10.1146/annurev.earth.050708.170910.

Royden, L. H., and D. J. Papanikolaou (2011), Slab segmentation and late Cenozoic disruption of the Hellenic arc, *Geochem. Geophys. Geosyst.*, *12*, Q03010, doi:10.1029/2010GC003280.

Sahu, H. S., M. J. Raab, B. P. Kohn, A. J. Gleadow, and K. D. Bal (2013), Thermal history of the Krishna-Godavari basin, India: Constraints from apatite fission track thermochronology and organic maturity data, *J. Asian Earth Sci.*, *73*, 1–20, doi:10.1016/j.jseaes.2013.04.028.

Sakellariou, D., and S. Dürr (1993), Geological structure of the Serbo-Macedonian massif in NE Chalkidiki peninsula [in Greek with English abstract], *Bull. Geol. Soc. Greece*, *XXVIII*(1), 179–193.

Sambridge, M., K. Gallagher, A. Jackson, and P. Rickwood (2006), Trans-dimensional inverse problems, model comparison and the evidence, *Geophys. J. Int.*, *167*(2), 528–542, doi:10.1111/j.1365-246X.2006.03155.x.

Sanchez, G., Y. Rolland, M. Jolivet, S. Brichau, M. Corsini, and A. Carter (2011), Exhumation controlled by transcurrent tectonics: The Argentera-Mercantour massif (SW Alps), *Terra Nova*, *23*(2), 116–126, doi:10.1111/j.1365-3121.2011.00991.x.

Schmidt, S., T. J. Nagel, and N. Froitzheim (2010), A new occurrence of microdiamond-bearing metamorphic rocks, SW Rhodopes, Greece, *Eur. J. Mineral.*, *22*, 189–198, doi:10.1127/0935-1221/2010/0022-1999.

Snel, E., M. Marunteanu, and J. E. Meulenkamp (2006), Calcareous nannofossil biostratigraphy and magnetostratigraphy of the upper Miocene and lower Pliocene of the Northern Aegean (Orphanic Gulf-Strimon Basin areas), Greece, *Palaeogeogr. Palaeoclimatol. Palaeoecol.*, *238*, 125–150, doi:10.1016/j.palaeo.2006.03.022.

Sokoutis, D., J.-P. Brun, J. van den Driessche, and S. Pavlides (1993), A major Oligo-Miocene detachment in southern Rhodope controlling north Aegean extension, *J. Geol. Soc. Lond.*, *150*, 243–246.

Soldatos, T., A. Koroneos, G. Christo des, and A. D. Moro (2001), Geochronology and origin of the Elatia plutonite (Hellenic Rhodope Massif, N. Greece) constrained by new Sr isotopic data, *N. Jb. Miner. Abh.*, *176*(2), 179–209.

Soldatos, T., A. Koroneos, B. K. Kamenov, I. Peytcheva, A. von Quadt, G. Christo des, X. Zheng, and H. Sang (2008), New U-Pb and Ar-Ar mineral ages for the Barutin-Buynovo-Elatia-Skaloti-Paranesti batholith (Bulgaria and Greece): Refinement of its debatable age, *Geochem., Mineral. Petrol.*, *46*, 85–102.

Stephenson, J., K. Gallagher, and C. Holmes (2006), Low temperature thermochronology and strategies for multiple samples: 2: Partition modelling for 2d/3d distributions with discontinuities, *Earth Planet. Sci. Lett.*, *241*(3–4), 557–570, doi:10.1016/j.epsl.2005.11.027.

Tompouloglou, C. (1981), Les minéralisations Tertiaires, type cuivre porphyrique, du Massif Serbo-Macédonien (Macédoine Grèce) dans leur contexte magmatique (avec un traitement géostatistique pour les donnees du prospect d'Alexia), PhD thesis, Ecole Nationale Superieure des Mines de Paris.

Tranos, M. D., E. E. Papadimitriou, and A. A. Kilias (2003), Thessaloniki-Gerakarou Fault Zone (TGFZ): The western extension of the 1978 Thessaloniki earthquake fault (Northern Greece) and seismic hazard assessment, *J. Struct. Geol.*, *25*(12), 2109–2123, doi:10.1016/S0191-8141(03)00071-3.

Tranos, M., A. Kilias, and D. Mountrakis (1999), Geometry and kinematics of the Tertiary post-metamorphic Circum Rhodope Belt Thrust System (CRBTS), northern Greece, *Bull. Geol. Soc. Greece*, *XXXIII*, 5–16.

Turpaud, P., and T. Reischmann (2010), Characterisation of igneous terranes by zircon dating: Implications for UHP occurrences and suture identification in the Central Rhodope, northern Greece, *Int. J. Earth Sci. (Geol Rundsch)*, *99*(3), 567–591, doi:10.1007/s00531-008-0409-x.

van Hinsbergen, D. J. J., E. Hafkenscheid, W. Spakman, J. E. Meulenkamp, and R. Wortel (2005), Nappe stacking resulting from subduction of oceanic and continental lithosphere below Greece, *Geology*, *33*(4), 325–328, doi:10.1130/G20878.1.

von Quadt, A., I. Peytcheva, S. Sarov, K. Naydenov, and N. Georgiev (2008), Metamorphic rocks from Dospat area of Western Rhodopes—Conventional and in situ U-Pb zircon dating, isotope tracing and correlations, in Bulgarian National Conference "GEOSCIENCES 2008".

von Quadt, A., S. Sarov, I. Peytcheva, and E. Voinova (2009), Jurassic metagranitoids south of the West-Rhodope batholith - conventional and in situ U-Pb zircon analyses, Sr-Nd-Hf isotope tracing and geodynamic constraints, in Bulgarian National Conference "GEOSCIENCES 2009".

Wang, X., M. Zattin, J. Li, C. Song, T. Peng, S. Liu, and B. Liu (2011), Eocene to Pliocene exhumation history of the Tianshui-Huicheng region determined by Apatite fission track thermochronology: Implications for evolution of the northeastern Tibetan Plateau margin, *J. Asian Earth Sci.*, *42*, 97–110, doi:10.1016/j.jseaes.2011.04.012.

Wawrzenitz, N., and A. Krohe (1998), Exhumation and doming of the Thasos metamorphic core complex (S Rhodope, Greece): Structural and geochronological constraints, *Tectonophysics*, *285*(3–4), 301–332, doi:10.1016/S0040-1951(97)00276-X.

Wuthrich, E. (2009), Low temperature thermochronology of the North Aegean Rhodope Massif, PhD thesis, Swiss Federal Institute of Technology, Zurich.

Yang, W., M. Jolivet, G. Dupont-Nivet, and Z. Guo (2013), Mesozoic-Cenozoic tectonic evolution of southwestern Tian Shan: Evidence from detrital zircon U/Pb and apatite fission track ages of the Ulugqat area, Northwest China, *Gondwana Res.*, doi:10.1016/j.gr.2013.07.020, in press.

Yi, Y., A. Carter, B. Xia, L. Ge, S. Brichau, and H. Xiaoqiong (2009), A fission-track and (U-Th)/He thermochronometric study of the northern margin of the South China Sea: An example of a complex passive margin, *Tectonophysics*, *474*(3–4), 584–594, doi:10.1016/j.tecto.2009.04.030.

Zagorchev, I. (1976), Tectonic, metamorphic and magmatic markers in the polycyclic ultra- metamorphic Ograzdenian complex, *Geol. Balc.*, *6*(2), 17–33.

Zervas, S. (1979), Age determination by the ^{87}Rb/^{87}Sr method of some pegmatites in the area of Lagada (Macedonia, Greece) [in Greek], *Ann. Geol. des Pays Helleniques*, *XXX*(1), 143–152.

Zidarov, N., I. Peytcheva, A. von Quadt, V. Andreichev, L. Macheva, and R. Titorenkova (2003), Timing and magma sources of metagranites from the Serbo-Macedonian Massif (Ograzhden and Maleshevska Mountains, SW Bulgaria): Constraints from U-Pb and Hf zircon and Sr whole rock isotope studies, in Bulgarian Geological Society, Annual Scientic Conference, Sofia, 11–12 Dec.

©2014. American Geophysical Union. All Rights Reserved.